

THE FATE OF DWARF GALAXIES IN CLUSTERS AND THE ORIGIN OF INTRACLUSTER STARS. I. ISOLATED CLUSTERS

PARAMITA BARAI,¹ WILLIAM BRITO,¹ AND HUGO MARTEL¹

Draft version November 28, 2018

ABSTRACT

The main goal of this paper is to compare the relative importance of destruction by tides, vs. destruction by mergers, in order to assess if tidal destruction of dwarf galaxies in clusters is a viable scenario for explaining the origin of intracluster stars. We have designed a simple algorithm for simulating the evolution of isolated clusters. The distribution of galaxies in the cluster is evolved using a direct gravitational N-body algorithm combined with a subgrid treatment of physical processes such as mergers, tidal disruption, and galaxy harassment. Using this algorithm, we have performed a total of 227 simulations. Our main results are (1) destruction of dwarf galaxies by mergers dominates over destruction by tides, and (2) the destruction of dwarf galaxies by tides is sufficient to explain the observed intracluster light in clusters.

Subject headings: cosmology — galaxies: clusters — galaxies: dwarfs — galaxies: interactions — methods: numerical

1. INTRODUCTION

1.1. Dwarf Galaxies

Dwarf galaxies (DGs) are the most numerous galaxies occurring in the Universe. A majority of galaxies in the local group are DGs (Mateo 1998). Also DGs comprise 85% of the Local Volume galaxy population ($D \leq 10$ Mpc, Karachentsev et al. 2004), and have been seen in observations of nearby galaxy clusters, Coma (Thompson & Gregory 1993; Bernstein et al. 1995), Virgo (Sandage et al. 1985; Impey et al. 1988; Phillipps et al. 1998; Lee et al. 2003), Fornax (Bothun et al. 1991; Drinkwater et al. 2003), Centaurus (Mieske et al. 2007), and several galaxy groups (Karachentseva et al. 1985; Ferguson & Sandage 1991; Côté et al. 1997; Carrasco et al. 2001; Cellone & Buzzoni 2005). DGs may have a space density ~ 40 times that of bright galaxies in the Universe (Staveley-Smith, Davies, & Kinman 1992).

DGs are defined as low-mass ($10^7 - 10^9 M_{\odot}$) galaxies having an absolute magnitude fainter than $M_B \sim -16$ mag, or $M_V \sim -18$ mag (Grebel 2001), have low surface brightness and low metallicity. Their small stellar fraction and very low luminosities make them the hardest galaxies to detect. They are believed to be the single systems with the largest proportion of dark-matter, and have a correspondingly high ratio of dark to luminous mass (e.g., Côté, Carignan, & Freeman 2000), with M/L ratios as high as that of galaxy groups and poor clusters. Due to their smaller masses and gravitational potentials, DGs are less able to retain their gas as compared to more massive galaxies, and in a clustered environment, the DGs are more likely to be disrupted by galactic encounters and environmental effects.

In the hierarchical clustering scenario of structure formation in the Universe (e.g., White & Frenk 1991; Kauffmann, White, & Guiderdoni 1993), the accretion of DGs causes the build up and growth of massive galax-

ies and large-scale structures. There exists a deficiency in the number of observed low-luminosity DGs (discrepancy more than one order of magnitude) as compared to the large number of theoretically predicted low-mass dark matter halos (e.g., Trentham & Tully 2002; Trentham, Tully, & Mahdavi 2006). This is recognized as a problem for cold dark matter theory, and the likely solution to this problem involves energy feedback from stellar evolution. Dense clusters are observed to contain a larger number of low-luminosity DGs per high-luminosity giant galaxy when compared to the field. Trentham & Hodgkin (2002) found that the Virgo cluster contains ~ 2.5 times more dwarf galaxies per giant galaxy when compared to the Ursa Major cluster. These imply that dwarfs are more common relative to giants in dense environments than diffuse ones.

The dynamical evolution of galaxies in a cluster is influenced by several mechanisms. There are two types of tidal interactions: the tidal forces due to other (massive) cluster galaxies (Gnedin 2003), and the tidal field resulting from the overall cluster potential (Merritt 1984; Byrd & Valtonen 1990). There can be collisions between the galaxies themselves due to their motion, sometimes resulting in mergers. Of particular interest is the occurrence of multiple high-velocity encounters between cluster galaxies (Richstone 1976), a phenomenon which is termed “galaxy harassment” (Moore et al. 1996). A phenomenon like tidal stirring (Mayer et al. 2001, where tidal shocks strip DGs) has a more pronounced effect on the less massive galaxies. There can also be stripping within galaxy groups and protoclusters accreting onto a cluster (Mihos 2004).

Works are found in the literature on the interaction of cluster environment with DGs in the cluster. Studying the core of the Fornax cluster, Hilker et al. (1999) examined a scenario in which DGs are accreted and dissolved at the cluster center. They found that the infall of DGs can largely explain many properties, but there are probably other physical processes occurring simultaneously, like the evolution of the more massive galaxies by stripping and merging. Mori & Burkert (2000) per-

¹ Département de physique, de génie physique et d’optique, Université Laval, Québec, QC, Canada

formed analytical and hydrodynamic studies of the interaction between the ICM of a cluster and an extended gas component of DGs surrounded by a cold dark matter halo. They found that the DG halos lose their diffuse gas rapidly by ram-pressure stripping in a typical cluster environment.

1.2. Intracluster Light

The diffuse intracluster light (ICL) observed in clusters of galaxies is produced by stars, usually of low surface brightness, located outside individual galaxies but within the cluster and associated with the cluster potential. The first mention of IC light was made by Zwicky (1951), who observed extended irregular regions of stars and low surface-brightness matter in the intergalactic spaces of the Coma cluster. Several observations have since detected diffuse light in galaxy clusters (e.g., Vilchez-Gomez 1999; Arnaboldi 2004, for reviews). Diffuse ICL has been observed in many galaxy cluster systems (e.g., Gonzalez et al. 2005; Krick et al. 2006), including non-cD galaxy clusters (e.g., Feldmeier et al. 2004a). Observations of diffuse ICL in Virgo (Mihos et al. 2005) reveal complex substructures in intricate web patterns including long tidal streamers, small tidal tails, and intergalactic bridges. The idea of IC globular clusters was proposed by West et al. (1995). Later on, distinct IC stars were observed, including globular clusters, red giant stars, and SN Ia (Gal-Yam et al. 2003). Individual IC stars have been found in Virgo (Ferguson et al. 1998; Arnaboldi et al. 2003), and Coma (Gerhard et al. 2005). Deep broadband imaging has helped to observe ICL in several other local galaxy clusters, e.g., Cantaurus, Fornax, Abell, and clusters up to intermediate redshifts. The origin and evolution of the IC stars and diffuse light are not well constrained at present.

Arguably these field stars are gravitationally stripped from their parent galaxies when the galaxies in a cluster interact dynamically with other galaxies or with the cluster potential. Continuous accumulation of ICL is now believed to be an ubiquitous feature of evolved galaxy clusters, with the unbound (i.e. intracluster) star fraction slowly increasing with time. From observations and cosmological simulations, at $z = 0$ at least 10 – 20% of all stars in a cluster are unbound to any one galaxy (e.g., Aguerri et al. 2005). As an upper limit, ICL constitute $\approx 10 - 40\%$ of a cluster’s luminosity. In observations and simulations, the fraction of stars in ICL increases with mass of the clusters, and increases with density of environment: from loose groups ($< 2\%$, Castro-Rodriguez et al. 2003), to Virgo-like (10%, Feldmeier et al. 2004b; Zibetti et al. 2005) and rich clusters ($\sim 20\%$ or higher, Tyson & Fischer 1995; Feldmeier et al. 2004a; Krick & Bernstein 2007). In the cores of dense and rich clusters (like Coma) the local ICL fraction can be as high as 50% (Bernstein et al. 1995).

The most popular formation mechanism of IC population is stripping of stars from cluster galaxies by gravitational tides, fast encounters between galaxies, and tidal interactions between colliding and merging galaxies (Miller 1983; Richstone & Malumuth 1983; Weil et al. 1997; Gregg & West 1998). Another contribution to the IC population can come from the infall of galaxy proto-clusters containing stars which are already unbound.

Studies of IC stars in the Virgo cluster (Feldmeier et al. 2004b) imply that bulk of the IC stars come from late-type galaxies and dwarf galaxies, and that the IC stars form by tidal stripping. Optical studies of ICL in intermediate redshift clusters (Zibetti et al. 2005) support that ICL is produced by stripping and disruption of galaxies when they pass through cluster centers. A dominant mechanism of ICL formation is believed to be tidal stripping during the hierarchical assembly of clusters.

Several authors have studied the origin of the diffuse ICL in clusters of galaxies using numerical simulation. Napolitano et al. (2003) performed high-resolution N-body Λ CDM simulations of a Virgo-like cluster to study the velocity and clustering properties of the IC stellar component at $z = 0$. The member galaxies in their simulated cluster undergo tidal interactions among themselves and with the cluster potential, to produce diffuse stars in the ICM. Their results substantially agree with the observed clustering properties of the diffuse IC stars in Virgo. Using hydrodynamical simulation of a $(192 h^{-1} \text{ Mpc})^3$ cosmological box, Murante et al. (2004) studied the statistical properties of IC stars in galaxy clusters and the dependence of the ICL properties on cluster mass and temperature. Their simulations reveal substantial (at least $\sim 10\%$) diffuse stellar light in a cluster, hidden from observations because of its very low surface brightness. Using high-resolution N-body + SPH simulations of a Coma-like cluster formed in a cosmological context, Willman et al. (2004) studied the formation, evolution and properties of IC stars in a rich cluster. Their results indicate that both massive and smaller galaxies contribute to ICL formation, with the stars stripped preferentially from the outer, lower-metallicity parts of a galaxy’s stellar distribution. The resulting fraction ($\sim 20\%$ at $z = 0$), and distribution of IC stars are in good agreement with the observed ICL properties. Sommer-Larsen et al. (2005) performed cosmological TREESPH simulations of the formation and evolution of galaxy groups and clusters, in order to discuss the ICL properties. They simulated a Virgo-like and a Coma-like cluster, and 4 galaxy groups, and predict several properties of IC stellar populations. Rudick et al. (2006) have used N-body simulations (done at both low and high resolutions) of the dynamical evolution of galaxy clusters to study the formation and evolution of the diffuse ICL component in 3 simulated galaxy clusters. They found that the ICL fraction of cluster luminosity increases as clusters evolve, reaching $\sim 10 - 15\%$ in evolved clusters.

In these numerical studies, there is always a trade-off between having good resolution or good statistics. Napolitano et al. (2003); Willman et al. (2004); Sommer-Larsen et al. (2005), and Rudick et al. (2006) simulate either one cluster or a few clusters, so even though their simulations have high resolution, they have poor statistics, in the sense that the cluster(s) they are simulating might not be representative of the whole cluster population. At the other extreme, Murante et al. (2004) simulate a very large cosmological volume, containing a statistically significant sample of clusters. Such large simulations however cannot resolve the scale of dwarf galaxies. Our goal is to have it both ways: achieving good statistics while resolving the processes responsible for destroying dwarf galaxies. This is achieved by

combining large-scale cosmological simulations with a semi-analytical treatment of mergers and tidal disruption.

1.3. Objectives

The main objective of the present work is to determine if dwarf galaxies in clusters are more prone to destruction by tides or to destruction by mergers. This determination is then used to predict the contribution of dwarf galaxies to the origin of intracluster stars in different types of cluster environments. The DGs in a cluster can be tidally disrupted (by the field of a more massive galaxy or by the background halo,) or the DGs can be destroyed when they merge with another galaxy. The impact of these two destruction mechanisms on the ICL is radically different. In the case of tidal disruption, the process contributes to IC stars in the cluster. In the case of merger, the DG is absorbed by a more massive galaxy, and there is essentially no contribution to the IC stars.

For the first part of this project, presented in this paper, we perform numerical simulations of isolated clusters of galaxies, in order to examine which method of dwarf galaxy destruction is dominant, and how the process depends on environmental factors. We identify six possible outcomes for our simulated galaxies: (1) the galaxy merges with another galaxy, (2) the galaxy is destroyed by the tidal field of a larger galaxy but the fragments accrete onto that larger galaxy, (3) the galaxy is destroyed by tides and the fragments are dispersed in the intracluster medium (ICM), contributing to the intracluster light, (4) the galaxy is destroyed by the tidal field of the background halo, (5) the galaxy survives to the present, and (6) the galaxy is ejected from the cluster.

We designed a simple algorithm to follow the evolution of galaxies in an isolated cluster. The gravitational interaction between galaxies is calculated by a direct N-body algorithm. The other physical mechanisms governing the possible outcomes (mergers, tidal disruption, accretion etc.) of the simulated galaxies are treated as “subgrid physics,” and are incorporated in the algorithm using a semi-analytical method. In the present work, we use this algorithm to simulate the evolution of isolated galaxy clusters, i.e. we assume that the cluster has already formed with its constituent galaxies in place, and it is neither accreting nor merging. Cluster accretion possibly has a finite impact on the evolution of dwarf galaxies, and on the origin of intracluster stars. In a forthcoming paper (Brito et al. 2008) we will address these issues by doing actual cosmological simulations over a statistically significant volume of the universe.

The remainder of this paper is organized as follows: In §2 we outline the numerical model for our galaxy clusters. The methodology of our simulations is described in §3. The results are presented in §4 and §5. We discuss the implications of our main goals in §6, and give our conclusions in §7.

2. THE NUMERICAL METHOD

2.1. The Basic PP Algorithm

We treat the system as an isolated cluster consisting of N galaxies of mass m_i , radius s_i , and internal energy U_i , orbiting inside a background halo of uncollapsed dark matter and gas. We assume that the halo is spherically

symmetric, and its radial density profile $\rho_{\text{halo}}(r)$ does not evolve with time (hence, we are neglecting infall motion that would result from cooling flows). Furthermore, we assume that the halo is stationary: it does not respond to the forces exerted on it by the galaxies, and therefore its center remains fixed at a point that we take to be the origin.

We represent each galaxy by *one single particle* of mass m_i . The “radius” s_i of the galaxy and its “internal energy” U_i are internal variables that only enter in the treatment of the subgrid physics described in §2.4 below. Our motivation for using this approach is the following: To simulate the destruction of dwarf galaxies by tides, it would seem more appropriate to simulate each galaxy using many particles. Supposing, however, that it takes at least 100 particles to properly resolve a dwarf galaxy experiencing tidal destruction, as the galaxies in our simulations cover 3 orders of magnitude in mass, the most massive ones would be represented by 100,000 particles. Even though the dwarf galaxies are much more numerous than the massive ones, the total number of particles would be above 1 million. This raises the following issues:

- With the use of tree codes, an $N = 10^6$ -particle simulation is not considered prohibitive anymore. However (1) our model has several free parameters, so we have a full parameter-space to study, and (2) one single cluster is not statistically significant, so for each combination of parameters we need to perform several simulations. For this paper, we performed 227 simulations. Doing 227 million-particle simulations would start to be computationally expensive.
- We could use unequal-mass particles, so that the most massive galaxies would not be represented by large numbers of particles. This is usually not a good idea. N-body simulations with particles having wildly different masses are known to suffer from all sorts of instability problems, which often require special algorithms to deal with. The approach we are considering here is more practical.
- In this paper, we consider isolated clusters. In a forthcoming paper (Brito et al. 2008), we will present simulations of a cosmological volume containing at least 100 clusters. The number of particles would then reach 100 million, and we would still need to explore the parameter space. This would be very computationally expensive. We will solve this problem using single-particle galaxies combined with a treatment of subgrid physics. The simulations presented in this paper can be seen as a test-bed for this approach.

The relatively small number of particles in our simulations (typically less than 1,000) enables us to use a direct, Particle-Particle (PP) algorithm, which is the simplest of all N-body algorithms. We took a standard PP code, which evolves a system of N gravitationally interacting particles using a second-order Runge-Kutta algorithm. We modified the original algorithm to include the interaction with the background halo, and we added several modules to deal with the subgrid physics. In this mod-

ified algorithm, the number of particles N can vary, as they merge, are destroyed by tides, or escape the cluster.

2.2. Gravitational Interactions

The acceleration of particle i (or galaxy i) is given by

$$\mathbf{a}_i = -G \sum_{j \neq i} \frac{m_j (\mathbf{r}_i - \mathbf{r}_j)}{(|\mathbf{r}_i - \mathbf{r}_j|^2 + \epsilon^2)^{3/2}} - \frac{GM_{\text{halo}}(r_i) \mathbf{r}_i}{(r_i^2 + \epsilon^2)^{3/2}}, \quad (1)$$

where \mathbf{r}_i and \mathbf{r}_j are the positions of particles i and j , respectively, m_j is the mass of particle j , $M_{\text{halo}}(r_i)$ is the mass of the background halo inside $r = r_i$, G is the gravitational constant, and ϵ is the softening length. This assumes that the background cluster halo is spherically symmetric and centered at the origin. In our PP algorithm, this expression is evaluated directly, by summing over all particles $j \neq i$. The softening length ϵ is chosen to be smaller than the initial radius of the smallest galaxies (see §3.2 below for the determination of the initial radius).

We evolve the system forward in time using a second-order Runge Kutta algorithm. The timestep Δt is calculated using

$$\Delta t = \min_i (\Delta t)_i, \quad (\Delta t)_i = \min \left[\frac{\epsilon}{|\mathbf{v}_i|}, \left(\frac{\epsilon}{|\mathbf{a}_i|} \right)^{1/2} \right], \quad (2)$$

where \mathbf{v}_i is the velocity of particle i , and we take the smallest value of $(\Delta t)_i$ to be the timestep Δt .

2.3. The Cluster Halo Density Profile

We consider two different types of density profile of the background halo of a cluster, $\rho_{\text{halo}}(r)$: the β profile, and the NFW profile.

In the first case, we assume that the dark matter in the background halo follows a similar density distribution as the observed intracluster gas. A single β -model (isothermal) density profile is used for the gas (e.g. King 1962; Cavaliere & Fusco-Femiano 1976; Makino, Sasaki, & Suto 1998),

$$\rho_{\text{gas}}(r) = \rho_0 \left[1 + (r/r_c)^2 \right]^{-3\beta/2}, \quad (3)$$

where, ρ_0 is the central density, and r_c is the core radius. The values of ρ_0 , r_c and β are taken from Piffaretti & Kaastra (2006), which gives the gas density parameters for 16 nearby clusters. The halo density is then obtained by scaling the gas density with the universal ratio of matter (dark + baryonic) to baryons, $\rho_{\text{halo}} = \rho_{\text{DM}} + \rho_{\text{gas}} = \rho_{\text{gas}} \Omega_M / \Omega_b$, where Ω_M and Ω_b are the present matter (baryons + dark matter) density parameter and baryon density parameter, respectively. This assumes that the cluster baryon mass fraction follows the cosmic value of Ω_b / Ω_M , which is expected to be generally true (e.g., White et al. 1993; Allen et al. 2002; Ettori 2003), although precise estimations of cluster baryon content have shown deviations from the universal value (Gonzalez et al. 2007, and references therein).

In a second case, we consider that the distribution of gas and dark matter in the background halo both follow analytical models of the dark matter density having a functional form

$$\rho_{\text{DM}}(r) = \frac{\rho_s}{(r/r_s)(1+r/r_s)^2} \quad (4)$$

(Navarro, Frenk, & White 1997). Here, ρ_s is a scaling density, and r_s is a scale length. The NFW profile is often parametrized in terms of a concentration parameter c . The parameters ρ_s and r_s are then given by

$$\rho_s = \frac{200c^3 \rho_{\text{crit}}(z)/3}{\ln(1+c) - c/(1+c)} = \frac{25H^2(z)c^3/\pi G}{\ln(1+c) - c/(1+c)}, \quad (5)$$

$$r_s = \frac{r_{200}}{c}, \quad (6)$$

where $\rho_{\text{crit}}(z) = 3H^2(z)/8\pi G$ is the critical density at formation redshift z , and r_{200} , the virial radius, is the radius of a sphere whose mean density is $200\rho_{\text{crit}}$ (200 times the critical density of the Universe at the epoch of formation). After scaling, the halo density profile is $\rho_{\text{halo}} = \rho_{\text{DM}} \Omega_M / (\Omega_M - \Omega_b)$.

Once we have chosen a particular density profile, the density is integrated to get the background cluster halo mass as

$$M_{\text{halo}}(r) = \int_0^r 4\pi x^2 \rho_{\text{halo}}(x) dx. \quad (7)$$

This is the mass that enters in the last term of equation (1). Since the density profiles we consider do not have an outer edge where $\rho_{\text{halo}} = 0$, we truncate the cluster background halo at a maximum halo radius $R_{\text{halo}}^{\text{max}} = 5 \text{ Mpc}$. Equation (7) is then solved numerically, to build an interpolation table for r in the range $[0, R_{\text{halo}}^{\text{max}}]$ that is then used by the code.

2.4. The Subgrid Physics

As mentioned in §1.3, there can be six possible physical outcomes for our simulated cluster galaxies. In the following subsections, we describe the associated subgrid physics for each mechanism we use in our simulations. The possible outcomes are: (1) the galaxy merges with another galaxy (§2.4.1), (2) the galaxy is destroyed by the tidal field of a larger galaxy but the fragments accrete onto that larger galaxy (§2.4.4), (3) the galaxy is destroyed by tides of a larger galaxy and the fragments are dispersed in the intracluster medium (§2.4.3), (4) the galaxy is destroyed by the tidal field of the background halo (§2.4.3), (5) the galaxy survives to the present (i.e., it is not destroyed by any process), and (6) the galaxy is ejected from the cluster (§2.4.5). We describe our approach of simulating galaxy harassment in §2.4.2.

2.4.1. Encounter: Merger

We simulate a pair of galaxies colliding (or synonymously, having an encounter) and the further consequences (e.g., merging) in the following way. An encounter is accounted for when two galaxies i and j , of radii s_i and s_j , overlap such that the center of the galaxy j is inside the galaxy i . Numerically the criterion is $r_{ij} < s_i$, where, $r_{ij} = |\mathbf{r}_i - \mathbf{r}_j|$ is the distance between the centers of the galaxies. If \mathbf{v}_i and \mathbf{v}_j are the velocities of galaxies i and j , the center of mass velocity of the pair is $\mathbf{v}_{\text{cm}} = (m_i \mathbf{v}_i + m_j \mathbf{v}_j) / (m_i + m_j)$. The kinetic energy in the center-of-mass rest frame is

$$K_{ij} = \frac{1}{2} m_i |\mathbf{v}_i - \mathbf{v}_{\text{cm}}|^2 + \frac{1}{2} m_j |\mathbf{v}_j - \mathbf{v}_{\text{cm}}|^2. \quad (8)$$

The gravitational potential energy of the pair is

$$W_{ij} = -\frac{Gm_i m_j}{r_{ij}}. \quad (9)$$

Even though we are treating each galaxy as a single particle, in reality a galaxy is a gravitationally bound system with an internal kinetic energy and a potential energy, and these energies must be included in the total energy of the interacting pair of galaxies. Considering a galaxy as a bound virialized system its internal energy is

$$U_i = U_{\text{potential}} + U_{\text{kinetic}} = \frac{U_{\text{potential}}}{2} = -\frac{\zeta G m_i^2}{2s_i}, \quad (10)$$

where ζ is a geometrical factor which depends on the mass distribution in the galaxies. Throughout this paper, we assume $\zeta = 1$ (see Appendix A).

We then compute the total energy of the galaxy pair (in the center of mass frame) as

$$E_{ij} = K_{ij} + W_{ij} + U_i + U_j. \quad (11)$$

If $E_{ij} \leq 0$, i.e., the system is bound, we then allow the galaxies to merge to form a single galaxy of mass $m_{\text{merge}} = m_i + m_j$. To compute its radius, we assume that energy is conserved, hence the total energy E_{ij} in the center-of-mass rest frame is all converted into the internal energy of the merger remnant. Its radius is then computed from equation (10),

$$s_{\text{merged}} = -\frac{\zeta G m_{\text{merge}}^2}{2U_{\text{merge}}} = \frac{\zeta G (m_i + m_j)^2}{2|E_{ij}|}. \quad (12)$$

The position and velocity of this merged object are set to those of the center-of-mass values of the galaxy pair before merger, in order to conserve momentum.

2.4.2. Encounter: Galaxy Harassment

In a high-speed encounter the two interacting galaxies come into contact for a brief amount of time. The galaxies might survive a merger or tidal disruption, but the encounter adds some internal energy into them, making them less bound. We refer to this process as *Galaxy Harassment*. This process has been originally suggested as a possible explanation for the origin of the morphology-density relation in clusters (Moore et al. 1996). We incorporate galaxy harassment in our algorithm by increasing the radius (or the internal energy) of a galaxy when it experiences a non-merger encounter. This enlargement makes a galaxy more prone to tidal disruption at a next encounter.

In equation (11), if $E_{ij} > 0$, i.e., the system is not bound, then the galaxies in our simulation do not merge in the collision. Rather a part of the kinetic energy of the galaxies is converted into internal energy, making the collision inelastic. We assume that an equal amount of energy is transferred to each galaxy. Denoting the energy transferred as ΔE , the kinetic energy of the pair decreases by ΔE , while the internal energy of each galaxy increases by $\Delta E/2$. We assume

$$\frac{\Delta E}{2} = \eta \min(|U_i|, |U_j|), \quad (13)$$

where η is an energy transfer efficiency whose value is taken as $\eta = 0.2$. The internal energies of the two galaxies after the encounter are $U_i^{\text{after}} = U_i^{\text{before}} + \Delta E/2$ and

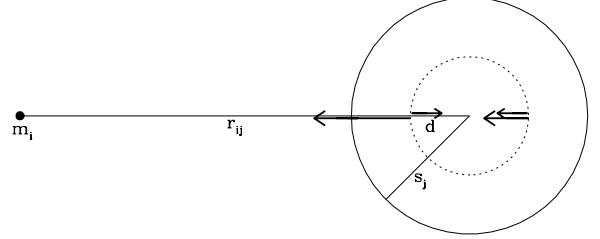


FIG. 1.— Calculation of the effects of tides caused by a galaxy of mass m_i on a galaxy of mass m_j and radius s_j . The two largest arrows show the gravitational accelerations caused by galaxy i ; the two smallest arrows show the accelerations caused by galaxy j . See §2.4.3 for details.

$U_j^{\text{after}} = U_j^{\text{before}} + \Delta E/2$, respectively. By choosing $\eta < 1$, we are ensuring that the internal energy of each galaxy remains negative, that is, the transfer of energy does not unbind the galaxies. We recalculate the velocities \mathbf{v}_i and \mathbf{v}_j after collision while conserving momentum, assuming that only the magnitudes of velocity change, the directions remaining the same. We recalculate the size of each galaxy in the pair using equation (12),

$$s_i^{\text{after}} = \frac{\zeta G m_i^2}{2|U_i^{\text{after}}|}, \quad s_j^{\text{after}} = \frac{\zeta G m_j^2}{2|U_j^{\text{after}}|}. \quad (14)$$

While allowing a size increase of the galaxies according to equations (12) and (14), we also considered a size cutoff. We assumed that the galaxies could grow only up to a maximum size given by the size of the largest galaxy at the beginning of the simulation.

2.4.3. Tidal Disruption: Intracluster Stars

We consider two possible sources of external gravitation for the tidal disruption of a galaxy j : another galaxy i , or the background cluster halo. The tidal force on a galaxy due to the gravitational field of the external source is meaningful only if the galaxy lies entirely on one side of the external source, when the tides are directed radially outwards tending to tear apart the galaxy. Our calculation of the tidal field caused by a galaxy i of mass m_i is illustrated in Figure 1. The galaxies i and j are separated by a distance r_{ij} . We calculate the resultant fields between two diametrically opposite points inside galaxy j , located at a radial distance $d \leq s_j$ along the line joining the centers of the two galaxies. The two small and two large arrows in Figure 1 indicate the gravitational field (or acceleration) at the opposite points caused by galaxy j (self-gravity) and by galaxy i (external source of gravitation), respectively. The magnitude of the tidal field is given by the difference between the gravitational field caused by galaxy i at the two opposite points,²

$$a_{\text{tide}}^{\text{galaxy}} = \frac{Gm_i}{(r_{ij} - d)^2} - \frac{Gm_i}{(r_{ij} + d)^2}. \quad (15)$$

The gravitational field caused by galaxy j (two small arrows in Figure 1) is directed radially inwards and acts opposite to the tides, tending to keep the galactic mass

² This reduces to the well-known form $a_{\text{tide}}^{\text{galaxy}} \propto d/r_{ij}^3$ in the limit $d \ll r_{ij}$, but we do not make this approximation here.

inside radius d intact. The difference between that self-gravitational field at the two opposite points is

$$a_{\text{grav}} = \frac{2Gm_j(d)}{d^2}, \quad (16)$$

where $m_j(d)$ is the mass of galaxy j inside radius d . When $a_{\text{tide}}^{\text{galaxy}} = a_{\text{grav}}$, then the tides will exceed self-gravity at radii larger than d , while self-gravity will exceed the tides at smaller radii. Thus the layers of galactic mass located between radii d and s_j would become unbound, while the ones located inside radius d would remain bound. Hence, the galaxy would be partly disrupted. In our code, we simplify things by using an “all-or-nothing” approach. A galaxy is either totally disrupted, or not disrupted at all. We consider that a galaxy is disrupted if half of its mass or more becomes unbound. If we assume an isothermal sphere density profile (as in Appendix A), then the half-mass radius is given by $d = s_j/2$. This is the value of d we use in equations (15) and (16). The criterion of tidal destruction then becomes $a_{\text{tide}}^{\text{galaxy}}(d) \geq a_{\text{grav}}(d)$, with $d = s_j/2$.

We also consider tidal disruption by the background cluster halo, but only if $r_j > s_j$ (that is, the galaxy does not overlap with the center of the halo). The magnitude of tidal field due to the cluster halo is

$$a_{\text{tide}}^{\text{halo}} = \frac{GM_{\text{halo}}(r_j - d)}{(r_j - d)^2} - \frac{GM_{\text{halo}}(r_j + d)}{(r_j + d)^2}, \quad (17)$$

where $M_{\text{halo}}(r)$ is given by equation (7). If $a_{\text{tide}}^{\text{halo}}(d) \geq a_{\text{grav}}(d)$, with $d = s_j/2$, galaxy j is tidally destroyed by the gravitational field of the halo.

When galaxy j is considered to have been tidally destroyed by another galaxy i , the fragments of the disrupted galaxy might accrete onto galaxy i (§2.4.4), or they might be dispersed into the ICM when $E_{ij} > 0$ [E_{ij} being the total energy of the galaxy pair given by eq. (11)]. For tidal destruction by the cluster halo the disrupted fragments are always dispersed into the ICM. In both cases, the destroyed galaxy is removed from the list of existing particles. The code keeps track of the amount of mass added to the ICM (in the form of IC stars) by tidal disruption. This quantity is initialized to zero at the beginning of the simulation, and every time a galaxy is tidally destroyed with its fragment dispersed, the mass of that galaxy is added up to the mass of IC stars.

2.4.4. Tidal Disruption: Accretion

We consider a possibility of accretion of the fragments of a tidally disrupted galaxy onto the galaxy causing the tides. This happens for the case of tidal disruption due to galaxies only (if the disruption is caused by the background cluster halo, the fragments are always dispersed as IC stars). This situation occurs when the conditions $a_{\text{tide}}^{\text{galaxy}} > a_{\text{grav}}$ and $E_{ij} \leq 0$ are both satisfied (see §2.4.3). The tidally disrupted galaxy accretes onto the more massive galaxy. The mass of the bigger galaxy increases from m_i to $m_i + m_j$. Thus a tidal disruption followed by accretion is similar to a merger (§2.4.1), but these events are counted separately.

2.4.5. Ejection

When a galaxy ventures at distances larger than the cluster halo truncation radius $R_{\text{halo}}^{\text{max}}$ (see §2.3), we consider that this galaxy has escaped from the cluster, and we remove it from the list. If we kept that galaxy, it might eventually return to the cluster. But in reality the universe contains many clusters, and a galaxy that moves sufficiently far away from one cluster will eventually feel the gravitational influence of other clusters, something that our algorithm, which simulates an isolated cluster, does not take into account. As we shall see, the ejection of galaxies from a cluster is quite uncommon in our simulations.

3. THE SIMULATIONS

3.1. Cosmological Model

We consider a Λ CDM model with the present matter density parameter, $\Omega_M = 0.241$, baryon density parameter, $\Omega_b = 0.0416$, cosmological constant, $\Omega_\Lambda = 0.759$, Hubble constant, $H_0 = 73.2 \text{ km s}^{-1} \text{ Mpc}^{-1}$ ($h = 0.732$), primordial tilt, $n_s = 0.958$, and CMB temperature, $T_{\text{CMB}} = 2.725 \text{ K}$, consistent with the results of WMAP3 (Spergel et al. 2007). Even though the simulations presented in this paper are not “cosmological” (we simulate isolated, virialized clusters), the particular choice of cosmological model enters the picture twice: in the determination of the radii of galaxies (see next section), and in the calculation of the elapsed time between the initial and final redshifts of the simulation.

In each simulation a cluster is evolved from $z = 1$ to the present ($z = 0$). We assume that the cluster will not experience any major merger during this period, and that, therefore, it is a good approximation to treat it as isolated. For our Λ CDM model, this represents a total evolutionary time of 7.63 Gyr.

3.2. Initial Conditions

To set the initial conditions of our simulations, we need to determine the initial mass m , radius s , position \mathbf{r} , and velocity \mathbf{v} of each galaxy. To determine the mass, we first assume that the luminosities of galaxies are distributed according to the Schechter luminosity function (Schechter 1976),

$$\phi(L)dL = \phi^* \left(\frac{L}{L^*} \right)^\alpha e^{-L/L^*} \frac{dL}{L^*}. \quad (18)$$

Here we use $L^* = 3.097 \times 10^{10} L_\odot$ (corresponding to absolute magnitude $M_{b,j}^* = -20.07$), and $\alpha = -1.28$, which is appropriate for galaxies located in clusters (De Propris et al. 2003). This luminosity function spans over $-22.5 < M_{b,j} < -15$. While it might be reasonable to assume fixed values of L^* and α , the value of ϕ^* most likely varies amongst clusters. So we normalize equation (18) by imposing that, in each cluster, there are N_0 galaxies with luminosities $L > L_0$. We use $N_0 = 25$, and $L_0 = 0.2L^*$ (corresponding to $M_b = -19$) (Lewis et al. 2002). We select the luminosities using a Monte Carlo rejection method. We then assume a constant mass-to-light ratio $\Upsilon = 193 h M_\odot/L_\odot = 73$ (Brainerd & Specian 2003), and convert the luminosities to masses. The Schechter function spans up to a maximum mass $M_{\text{max}} = 220 \times 10^{11} M_\odot$. To generate the dwarf galaxies, the same Schechter function is extrapolated up to a minimum mass $M_{\text{min}} = 1 \times 10^9 M_\odot$.

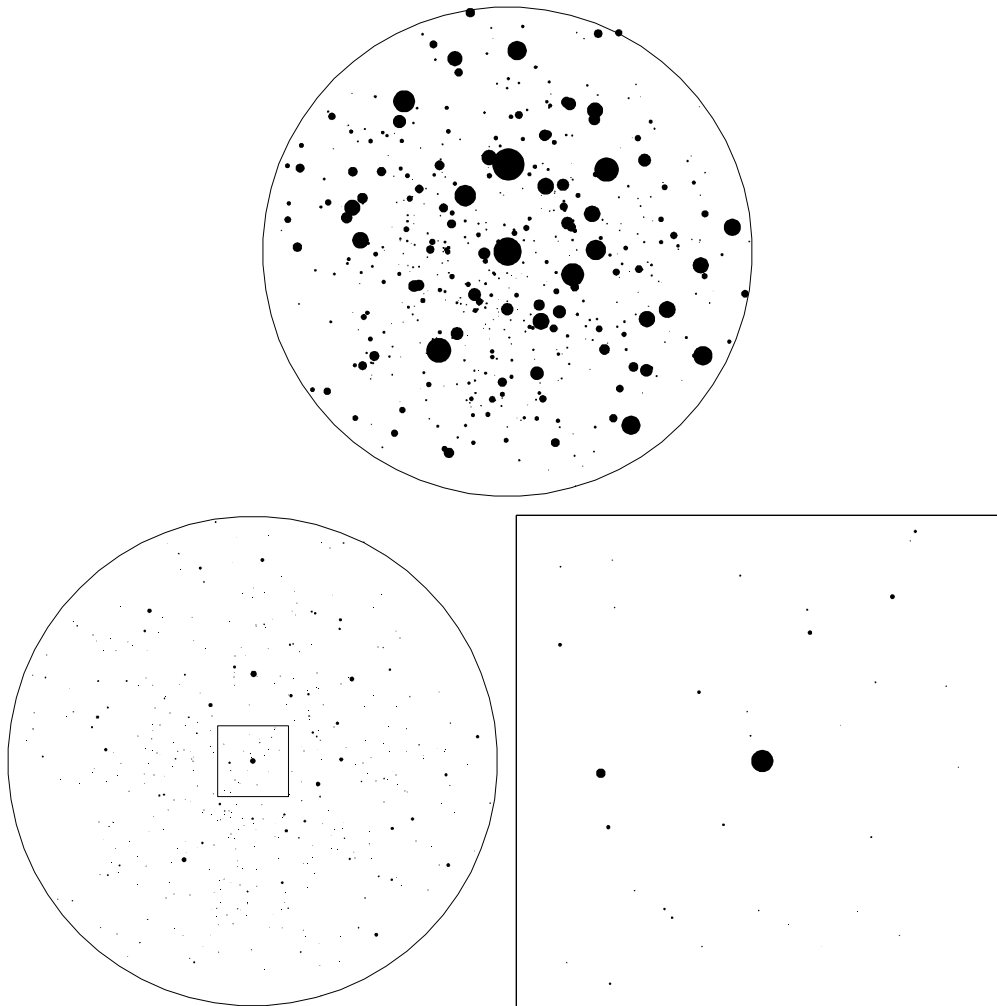


FIG. 2.— Initial conditions for run A12. Top panel: initial conditions at $z = 1$. The solid circles indicate the virial radii of galaxies. The large circle is the maximum distance $r = 3R_0 = 2.08$ Mpc from the cluster center. Lower left panel: same as top panel, with symbols rescaled to optical diameter of real galaxies. Bottom right panel: enlargement of the central $(0.6 \text{ Mpc})^2$, (box on lower-left panel).

We take the radius s of each galaxy to be equal to the virial radius r_{200} (radius containing matter with 200 times the mean density of the Universe at the epoch of galaxy formation) corresponding to the galaxy mass $m = M_{200}$ using

$$M_{200} = \frac{800\pi}{3} r_{200}^3 \bar{\rho} (1 + z_{\text{coll}})^3. \quad (19)$$

Here, $\bar{\rho} = \rho_{\text{crit}} \Omega_M = 3H_0^2 \Omega_M / 8\pi G$ is the mean matter density in the present universe, and z_{coll} is the redshift of collapse when the galaxy formed. To obtain z_{coll} , we use a simple spherical collapse model. First, by filtering the power spectrum for our Λ CDM model, we calculate the standard deviation $\sigma(m)$ of the linear density contrast $\delta = (\rho - \bar{\rho}) / \bar{\rho}$ at the mass scale m . The distribution of the values of δ is then given by a Gaussian,

$$\mathcal{P}(\delta) \propto \exp\left(-\frac{\delta^2}{2\sigma^2}\right). \quad (20)$$

We pick randomly a present density contrast $\delta_0 = \delta(z = 0)$ from this distribution, using a Monte Carlo rejection method, and solve the following equation to get the collapse redshift z_{coll} ,

$$\Delta_c = \delta_0 \frac{\delta_+(z_{\text{coll}})}{\delta_+(0)}, \quad (21)$$

where $\delta_+(z)$ is the linear growing mode (for $\Lambda \neq 0$ models, see, e.g., Martel 1991). Here, $\Delta_c = 3(12\pi)^{2/3}/20 = 1.686$ is the overdensity predicted by linear theory at recollapse. We solve this equation numerically for z_{coll} , and substitute the solution in equation (19), which we then solve to get the radius $s = r_{200}$.

To determine the locations of galaxies inside a cluster, we assume that their distribution is isotropic (in a statistical sense). We can therefore choose the spherical coordinates (θ, ϕ) of each galaxy randomly, using $\phi = 2\pi X_\phi$,

and $\cos\theta = 2X_\phi - 1$, where X_ϕ and X_θ are random numbers drawn from a uniform deviate between 0 and 1. We still need to determine the radial coordinate r . Using the CNOC cluster survey, Carlberg et al. (1997) showed that the radial mass density $\rho(r)$ of matter and the radial number density $\nu(r)$ of galaxies are roughly proportional to each other, where both $\rho(r)$ and $\nu(r)$ are approximated by NFW profiles. Girardi et al. (1998) found that the halo mass follows the galaxy distribution in clusters, using a β -model for the halo/galaxy volume density profile. We assume that this proportionality holds for all clusters, and we generalize it to all the density profiles we use. Thus, the assumed background halo mass density profile [eqs. (3) and (4)] gives us $\nu(r)$. We can then select the initial distances r from the cluster center using again a Monte Carlo rejection method. Since the masses and locations of the galaxies have been determined separately, we need to pair them, that is, for each selected location, to decide which galaxy goes there. We do expect the most massive galaxies to reside near the center of the cluster. However, low-mass galaxies are not all located at large radii, and some of them might be located in the central region of the cluster as well. Indeed, if the galaxies in the central region were all massive, it would be impossible to reproduce the desired number density profile $\nu(r)$ and not have the galaxies overlap.

To prevent any overlap, we locate the galaxies as follows: we first position the most massive galaxy at the center of the cluster. Then we locate the next 7 most massive galaxies between radii R_0 and $2R_0$, where R_0 is 3 times the radius of the most massive galaxy. We then locate the next 19 most massive galaxies between radii $2R_0$ and $3R_0$. Finally, the remaining galaxies are located randomly between radii 0 and $3R_0$. During the process we check that the galaxies do not overlap, by ensuring that the distance between the edges of two galaxies is greater than the radius of the larger galaxy, i.e., $r_{ij} - s_i - s_j > \max(s_i, s_j)$. In the process of locating a galaxy, if this criterion is not satisfied, we simply reject that location and generate a new one.

After assigning the masses, radii, and positions of all the galaxies, we determine the velocity of each galaxy. We consider the velocity a galaxy would have if it were in a perfect circular orbit at radius r ,

$$v_{\text{circ}}(r) = \left[\frac{G}{r} \left(M_{\text{halo}}(r) + \sum_{j, r_j < r} m_j \right) \right]^{1/2}, \quad (22)$$

where the sum only includes galaxies inside radius r . The norm of the velocity is chosen by giving a random 10% deviation to the circular velocity, i.e., $v = v_{\text{circ}}(1 + 0.1X_v)$, where X_v is a random number between -1 and 1 . For the direction of the velocity, we follow a similar random angle generation technique as we did for the positions of galaxies.

Figure 2 illustrates the initial conditions for one of our simulations (run A12). The top panel shows the cluster at $z = 1$. The large circle represents the maximum distance $3R_0$ within which the galaxies are located initially. Each dot represents a galaxy, with the most massive one located in the center. Even though massive galaxies tend to be larger, there is no direct correspondence between the masses and radii because of the dependence on z_{coll}

in equation (19), whose determination involves a Monte Carlo method.

Visually, this looks quite different from the optical pictures of actual clusters like Virgo. This is because each dot has a radius s equal to the virial radius r_{200} , that can exceed the optical radius by an order of magnitude. In the bottom left panel of Figure 2, we show the same cluster, with all the dots rescaled in size so that the angular diameter of the central galaxy is equal to $8.3'$ at a distance of 16.8 Mpc, which is the observed optical diameter of M87. The bottom right panel shows a zoom-in of the central cluster region. It looks qualitatively similar to pictures of the central region of Virgo.

4. RESULTS

We started by performing 9 series of simulations, for a total of 132 simulations. Table 1 summarizes the characteristics of each series. The first 2 columns show the series name and the number of runs, respectively. The slope of the Schechter luminosity function at $z = 1$ (used to generate the initial conditions) is listed in column 3. Columns 4 to 8 give the characteristics and relevant parameter values of the background cluster halo profile. Columns 9 and 10 indicate respectively whether a cD galaxy was included in the cluster simulation, and whether galaxy harassment was included as part of the subgrid physics.

4.1. Series A: Initial Simulations

We performed an initial series of 16 simulations, using for the background halo a β -profile with $\beta = 0.33$, a core radius $r_c = 3$ kpc, and a central density $\rho_0 = 8.14 \times 10^{-26} \text{ g cm}^{-3}$, which is appropriate for a cluster like Virgo (Piffaretti & Kaastra 2006). For this series, we did not include galaxy harassment. Our results are shown in Table 2. It shows the run number (column 1), and, at the beginning of the run, the total mass M_{total} in galaxies, in units of $10^{11} M_\odot$ (column 2), the number of galaxies N_{total} (column 3), and the Schechter luminosity function [eq. (18)] exponent α_{start} (column 11). This exponent was obtained by performing a numerical fit to the distribution of galaxy masses. Because the masses were determined from a Monte Carlo rejection method, the exponent can differ from the intended value $\alpha = -1.28$ in equation (18) and listed in Table 1, but the deviations are small. Averaging over all runs, we get

$$\alpha_{\text{start}} = -1.280 \pm 0.020. \quad (23)$$

Columns 4 – 8 in Table 2 show the number of galaxies N_{merge} destroyed by mergers, the number of galaxies $N_{\text{tides}}^{\text{gal}}$ destroyed by tides caused by a massive galaxy, with the fragments dispersed in the ICM, the number of galaxies N_{accr} destroyed by tides caused by a massive galaxy, with the fragments being accreted onto that galaxy, the number of galaxies $N_{\text{tides}}^{\text{halo}}$ destroyed by the tidal field of the background halo, and the number of galaxies N_{eject} ejected from the cluster, respectively. Column 9 shows the fraction *by numbers* of galaxies f_{surv} that survive to the present.

We did not find a single occurrence of a galaxy destroyed by tides from the background halo, and the number of galaxies ejected is either 0 or 1. There are large variations in the other numbers from one run to the next,

TABLE 1
SERIES OF SIMULATIONS

Series	Runs	α_{start}	profile	β	ρ_0, ρ_s [g cm^{-3}]	c	r_c, r_s [kpc]	cD	Harassment
A	16	-1.28	β -Virgo	0.33	8.14×10^{-26}	...	3	×	×
B	17	-1.28	β -Virgo	0.33	8.14×10^{-26}	...	3	×	✓
C	17	-1.36	β -Virgo	0.33	8.14×10^{-26}	...	3	×	✓
D	16	-1.36	β -Virgo	0.33	8.14×10^{-26}	...	3	✓	✓
E	16	-1.36	β -Perseus	0.53	7.27×10^{-26}	...	28	×	✓
F	16	-1.36	β -Perseus	0.53	7.27×10^{-26}	...	28	✓	✓
G	10	-1.28	NFW	...	2.35×10^{-25}	5	200	×	✓
H	14	-1.31	NFW	...	2.35×10^{-25}	5	200	×	✓
I	10	-1.31	NFW	...	2.35×10^{-25}	5	200	✓	✓

TABLE 2
SIMULATIONS FOR SERIES A

Run	$M_{\text{total}}[10^{11} M_{\odot}]$	N_{total}	N_{merge}	$N_{\text{tides}}^{\text{gal}}$	N_{accr}	$N_{\text{tides}}^{\text{halo}}$	N_{eject}	f_{surv}	f_{ICS}	α_{start}	α_{end}
A1	855.0	440	137	54	6	0	1	0.550	0.225	-1.26	-1.23
A2	862.0	702	343	182	24	0	1	0.217	0.490	-1.28	-1.12
A3	1100.4	480	126	43	7	0	0	0.633	0.136	-1.28	-1.24
A4	831.0	530	165	67	11	0	0	0.542	0.148	-1.26	-1.15
A5	980.4	459	175	58	8	0	1	0.473	0.128	-1.25	-1.18
A6	967.8	640	230	74	5	0	0	0.517	0.157	-1.29	-1.23
A7	720.0	579	263	114	7	0	0	0.337	0.359	-1.28	-1.20
A8	757.8	435	200	66	51	0	1	0.269	0.320	-1.27	-1.26
A9	925.6	514	223	83	12	0	1	0.379	0.245	-1.28	-1.17
A10	858.9	525	204	54	8	0	0	0.493	0.257	-1.31	-1.24
A11	880.2	547	224	68	9	0	1	0.448	0.257	-1.33	-1.25
A12	826.1	548	255	72	15	0	1	0.374	0.225	-1.29	-1.18
A13	1041.5	431	166	51	6	0	0	0.483	0.275	-1.27	-1.25
A14	957.3	486	174	52	4	0	0	0.527	0.261	-1.29	-1.22
A15	860.5	520	160	64	15	0	1	0.538	0.260	-1.26	-1.18
A16	858.0	483	255	72	8	0	0	0.306	0.323	-1.28	-1.19

but some trends are apparent. Typically, 50% to 60% of the galaxies are destroyed. Run A2 is an extreme case, with 78% of the galaxies being destroyed. The destruction of galaxies by mergers dominates over the destruction by tides, by more than a factor of 2 except for run A7. If we treat the cases of tidal disruption followed by accretion as being mergers, then mergers dominate even more over tidal disruption. When galaxies are destroyed by tides, the dispersion of fragments into the ICM always dominates over the accretion of fragments onto the massive galaxy, but the ratio varies wildly, from 114:7 in run A7 to 66:51 in run A8.

We can now evaluate the fraction f_{ICS} of the total luminosity of the cluster that comes from intracluster stars. Since we assume a constant mass-to-light ratio, this fraction is given by

$$f_{\text{ICS}} = \frac{M_{\text{tides}}^{\text{gal}} + M_{\text{tides}}^{\text{halo}}}{M_{\text{total}} - M_{\text{eject}}}. \quad (24)$$

where the letter M refers to the mass in galaxies, rather than their number. The galactic mass contribution to the ICM consists of galaxies destroyed by tides of another more massive galaxy, and by tides of the background halo (though there are no such cases in this series).

The values of f_{ICS} are listed in column 10 of Table 2. Again, there are large variations. In particular, the fraction is very large for run A2, and very small for runs A3

and A5. Averaging over all runs, we get

$$f_{\text{ICS}} = 0.254 \pm 0.093. \quad (25)$$

Even though, in most cases about half the number of galaxies are destroyed, they tend to be low-mass galaxies, which explains why $f_{\text{ICS}} < 1 - f_{\text{surv}}$, for all the runs.

The galaxies being destroyed by mergers and tides, or escaping are mostly low-mass galaxies. This leads to a flattening of the galaxy mass distribution function. We computed the best numerical fit to the Schechter luminosity function exponent α [eq. (18)] for the surviving galaxies at the end of the simulations. This is listed as α_{end} in column 12 of Table 2. Averaging over all runs, we get

$$\alpha_{\text{end}} = -1.206 \pm 0.040. \quad (26)$$

4.2. Series B: Turning on Harassment

We modified the algorithm to include the effect of galaxy harassment (see §2.4.2), and rerun the calculations of series A with the same initial conditions. We also added one more run, B17. The results are shown in Table 3, which follows the same format as Table 2. Comparing with series A, the number of galaxies destroyed by mergers is very similar, but the number of galaxies destroyed by tides tends to be significantly higher. For instance, it goes from 67 to 94 for runs A4-B4, and from 64 to 86 for runs A15-B15. This is because, when a galaxy is subjected to harassment, its binding energy is reduced,

TABLE 3
SIMULATIONS FOR SERIES B

Run	$M_{\text{total}}[10^{11}M_{\odot}]$	N_{total}	N_{merge}	$N_{\text{tides}}^{\text{gal}}$	N_{accr}	$N_{\text{tides}}^{\text{halo}}$	N_{eject}	f_{surv}	f_{ICS}	α_{start}	α_{end}
B1	855.0	440	134	62	6	0	1	0.539	0.237	-1.26	-1.24
B2	862.0	702	337	210	25	0	1	0.184	0.454	-1.28	-1.11
B3	1100.4	480	126	48	7	0	0	0.623	0.139	-1.28	-1.24
B4	831.0	530	159	94	12	0	0	0.500	0.184	-1.26	-1.15
B5	980.4	459	171	78	7	0	1	0.440	0.154	-1.25	-1.21
B6	967.8	640	226	85	6	0	0	0.505	0.173	-1.29	-1.23
B7	720.0	579	249	134	9	0	0	0.323	0.364	-1.28	-1.20
B8	757.8	435	172	79	62	0	1	0.278	0.271	-1.27	-1.27
B9	925.6	514	223	100	12	0	1	0.346	0.270	-1.28	-1.19
B10	858.9	525	206	68	7	0	0	0.465	0.298	-1.31	-1.25
B11	880.2	547	233	85	9	0	1	0.400	0.280	-1.33	-1.27
B12	826.1	548	241	92	19	0	1	0.356	0.240	-1.29	-1.20
B13	1041.5	431	160	58	4	0	0	0.485	0.269	-1.27	-1.26
B14	957.3	486	173	59	5	0	0	0.512	0.274	-1.29	-1.22
B15	860.5	520	155	86	17	0	1	0.502	0.277	-1.26	-1.19
B16	858.0	483	264	90	6	0	0	0.255	0.354	-1.28	-1.16
B17	792.6	451	178	83	16	0	1	0.384	0.346	-1.24	-1.13

and it becomes more prone to experience tidal disruption later. The number of tidal disruptions followed by accretion does not change significantly, though. Hence, the additional, tidally-disrupted galaxies almost all contribute to the intracluster stars. The values of f_{ICS} are therefore increased relative to series A. The mean value is

$$f_{\text{ICS}} = 0.269 \pm 0.081. \quad (27)$$

This is not significantly larger than for series A. The additional galaxies destroyed are mostly low-mass galaxies. We also recalculated the best-fit Schechter exponent α for the surviving galaxies at $z = 0$. The mean value for the runs in this series is

$$\alpha_{\text{end}} = -1.207 \pm 0.048. \quad (28)$$

Figure 3 shows the total galaxy counts in mass bins, obtained by combining all the runs in series B, along with the fitting curves to a Schechter distribution function [eq. (18)]. The best fit Schechter exponent for the initial galaxy distribution (the upper curve at $z = 1$) is $\alpha = -1.28$, and for the final surviving galaxy distribution (the lower curve at $z = 0$) is $\alpha = -1.20$. These values of α were obtained by performing the numerical Schechter function fits on the combined set of galaxies taken from all the 17 runs in this series, which amounts to 8770 initial galaxies at $z = 1$ and 3614 surviving galaxies at $z = 0$.

Clearly from Figure 3, the fit at $z = 0$ (lower curve) is excellent. This shows that, in our simulations, a Schechter mass (luminosity) distribution function at $z = 1$ remains a Schechter distribution all the way to $z = 0$, though half of the galaxies are destroyed. Only the slope α changes with time.

4.3. Series C: Steeping up the Mass Distribution Function

In the simulations of series A and B, the Schechter exponent α evolves from $\alpha \simeq -1.28$ at $z = 1$ to $\alpha \simeq -1.21$ at $z = 0$. Analyzing the combined set of galaxies of all the 17 runs in series B, we obtained the best fit Schechter exponent for the surviving galaxy distribution at $z = 0$ as $\alpha = -1.20$. This is a problem, since the value of

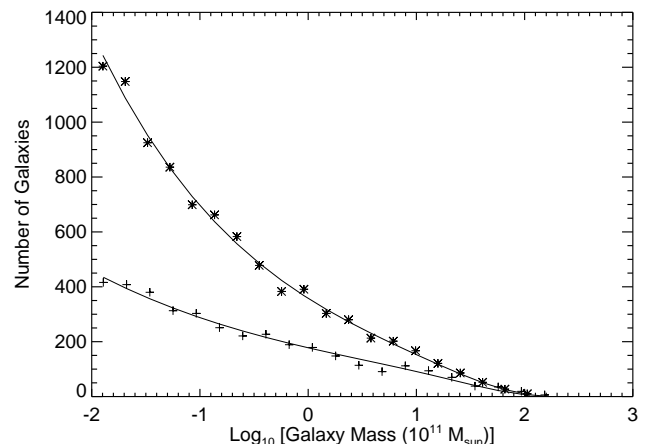


FIG. 3.— Mass distribution function for galaxies in Series B, obtained by adding the numbers for all runs. Results are plotted for initial 8770 galaxies at $z = 1$ (asterisks) and surviving 3614 galaxies at $z = 0$ (plus signs). The curves show the best fit of a Schechter distribution function (eq. 18), with $\alpha = -1.28$ at $z = 1$ (upper curve), and $\alpha = -1.20$ at $z = 0$ (lower curve).

$\alpha = -1.28$ is based on observations of nearby clusters (De Propris et al. 2003), and should be valid for clusters of galaxies at $z = 0$, whereas we used the same $\alpha = -1.28$ to start our simulations at $z = 1$, and it flattened to $\alpha = -1.20$ at $z = 0$. Ryan et al. (2007) recently determined the luminosity function of a large sample of galaxies at $z \simeq 1$, and concluded that there is a steepening of the faint-end slope with redshift, which is expected in the hierarchical formation scenario of galaxies. They obtained a value of the faint-end slope $\alpha = -1.32 \pm 0.07$ at $z = 1$.

In our simulations we take into account this flattening of the luminosity function over time as explained below. The results of series A and B suggest that $|\alpha|$ decreases by ~ 0.08 between $z = 1$ and $z = 0$. Using this as a guide, we performed a new series of simulations, series C, using $\alpha_{\text{start}} = -1.36$, with the hope that this value will evolve toward something close to $\alpha = -1.28$ at $z = 0$. The results are shown in Table 4. The average values of

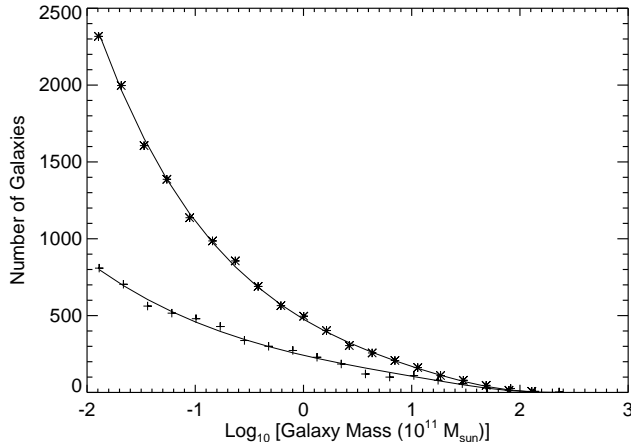


FIG. 4.— Same as Figure 3, for series C. Results are plotted for initial 13628 galaxies at $z = 1$ (asterisks) and surviving 5356 galaxies at $z = 0$ (plus signs). The best fit Schechter distribution functions are with $\alpha = -1.36$ at $z = 1$ (upper curve), and $\alpha = -1.27$ at $z = 0$ (lower curve).

α are

$$\alpha_{\text{start}} = -1.357 \pm 0.021, \quad (29)$$

$$\alpha_{\text{end}} = -1.272 \pm 0.050. \quad (30)$$

Figure 4 (analogous to Figure 3) shows that at $z = 0$, a Schechter distribution function is still a good approximation to the mass distribution. Combining the galaxies from all the 17 runs in this series (13628 initial galaxies at $z = 1$, and 5356 surviving galaxies at $z = 0$), the best fit Schechter exponent for the initial galaxy distribution (the upper curve) is $\alpha = -1.36$, and for the surviving galaxy distribution (the lower curve) is $\alpha = -1.27$. This value of α is close enough to our target value of -1.28 . So from now on, in all subsequent series with the β model halo density profile, we will use an initial α of -1.36 , as shown in Table 1. This value is well inside the range obtained by Ryan et al. (2007).

Using a steeper galaxy distribution while still requiring that the clusters contain 25 galaxies with $L > 0.2L_*$ (see initial conditions in §3.2) results in the initial number of galaxies being larger by a factor of about 2 (column 3 of Table 4). But the numbers of galaxies destroyed by mergers and tides are also higher relative to series B. As a result the trends are similar. In particular, mergers still dominate over tides by more than a factor of 2.

The run C1 has a larger number of galaxies ejected from the cluster. This is because the most massive galaxy, located at the center of the cluster, was particularly large. Its radius was $s = 385$ kpc, compared to $s \lesssim 300$ kpc for the other runs. This increased the value of R_0 (see §3.2) used for setting up the initial conditions. As a result, more galaxies were located at larger radii, where they are more likely to escape.

The mean value of f_{ICS} for this series is

$$f_{\text{ICS}} = 0.284 \pm 0.090. \quad (31)$$

4.4. Series D: Adding a cD Galaxy

A cD (*central dominant*) galaxy is a very bright supergiant elliptical galaxy with an extended envelope (or a

diffuse halo) found at the center of a cluster (Schombert 1988). Several galaxy clusters have been found to have cD galaxies at their centers (e.g., Quintana & Lawrie 1982; Hill & Oegerle 1998; Oegerle & Hill 2001; Jordan et al. 2004; Seigar, Graham, & Jerjen 2007). We performed some simulations by incorporating a cD galaxy in the clusters. Being the brightest and most massive cluster galaxy, the mass of a cD is larger than the prediction of the normal Schechter distribution function (eq. 18). So we introduced the cD galaxy manually at our simulated cluster center. We adopted a luminosity of $L_{\text{cD}} = 10L_*$, which is a canonical value for a cD. Using our mass to light ratio ($\Upsilon = 193 h M_{\odot}/L_{\odot}$, §3.2), this corresponds to a cD galaxy mass of $M_{\text{cD}} = 437.6 \times 10^{11} M_{\odot}$. When we wanted a cD galaxy present in the simulation we changed the mass of the cluster central galaxy (see §3.2) to the cD mass, M_{cD} . This allowed us to keep the appropriate initial galaxy distribution for a cluster while incorporating a cD galaxy at rest, located at the center.

We performed simulations by adding a cD galaxy to our Virgo-like cluster, and called it series D. The results are listed in Table 5, from which certain trends are clear after incorporating a cD galaxy in the simulation. The total galaxy mass increases since a massive cD galaxy is being added. More prominent than in the previous series A, B, and C, here galaxy mergers outnumber tides by factors $\sim 2 - 3$, which go as high as 4 in run D12.

A striking new feature in cases incorporating a cD galaxy is the increase in the number of accretions after tidal disruption by a galaxy, fully 1/4 of the galaxies being accreted in run D5. Since in these accretions, the smaller galaxy is tidally destroyed and is absorbed (or merged) by the massive galaxy (§2.4.4), it appears, in our simulated clusters, that in the presence of a cD galaxy the number of effective mergers is very high.

The mass fraction imparted to ICS has decreased in all the runs, with a value as low as 0.065 in run D6. To explain such a result, we note that the most massive central galaxy (cD or otherwise) in our simulated cluster is never destroyed because of its large mass. In an encounter, it is normally the lower-mass galaxy that gets destroyed. Also the initial conditions of the most massive galaxy (at rest at the center, see §3.2) make it less likely to be destroyed by the tidal field of the halo. If the central galaxy is a cD, a large mass fraction (as high as 38% in run D11) is locked into it, which can never contribute to the ICS. So a smaller mass fraction is available to be transferred to the ICS, which eventually leads to a decrease in f_{ICS} .

The mean value of f_{ICS} for series D is

$$f_{\text{ICS}} = 0.124 \pm 0.036. \quad (32)$$

4.5. Series E & F: Other β Profiles

In the next two series of runs, we consider a different background halo. We use a β -profile with $\beta = 0.53$, a core radius $r_c = 28$ kpc and a central density $\rho_0 = 7.27 \times 10^{-26} \text{ g cm}^{-3}$, which is appropriate for a cluster like Perseus (Piffaretti & Kaastra 2006). Series E and F do not include, and include a cD galaxy, respectively (hence series E should be compared with series C, and series F with series D).

The results for series E are shown in Table 6. The

TABLE 4
SIMULATIONS FOR SERIES C

Run	$M_{\text{total}}[10^{11} M_{\odot}]$	N_{total}	N_{merge}	$N_{\text{tides}}^{\text{gal}}$	N_{accr}	$N_{\text{tides}}^{\text{halo}}$	N_{eject}	f_{surv}	f_{ICS}	α_{start}	α_{end}
C1	1144.3	948	322	123	13	0	7	0.509	0.162	-1.34	-1.27
C2	1009.9	936	283	138	19	0	1	0.529	0.195	-1.38	-1.30
C3	914.2	603	316	97	13	0	0	0.294	0.265	-1.35	-1.24
C4	970.5	635	162	86	11	0	1	0.591	0.216	-1.32	-1.28
C5	935.9	672	250	101	7	0	1	0.466	0.158	-1.33	-1.25
C6	948.2	1136	502	268	6	0	0	0.317	0.318	-1.35	-1.21
C7	926.4	884	276	155	10	0	1	0.500	0.258	-1.35	-1.28
C8	818.4	696	347	142	62	0	1	0.207	0.423	-1.35	-1.26
C9	875.9	903	421	255	44	0	1	0.202	0.405	-1.34	-1.19
C10	1110.5	785	286	100	20	0	1	0.482	0.168	-1.39	-1.39
C11	864.2	809	338	139	18	0	1	0.387	0.386	-1.40	-1.36
C12	1053.2	978	395	212	29	0	0	0.350	0.294	-1.36	-1.29
C13	1151.7	790	344	127	24	0	1	0.372	0.262	-1.37	-1.29
C14	876.8	684	335	133	23	0	1	0.281	0.320	-1.37	-1.21
C15	788.0	769	240	140	27	0	0	0.471	0.243	-1.35	-1.26
C16	905.1	578	284	80	24	0	1	0.327	0.430	-1.36	-1.29
C17	889.2	822	325	169	13	0	0	0.383	0.323	-1.36	-1.25

TABLE 5
SIMULATIONS FOR SERIES D

Run	$M_{\text{total}}[10^{11} M_{\odot}]$	N_{total}	N_{merge}	$N_{\text{tides}}^{\text{gal}}$	N_{accr}	$N_{\text{tides}}^{\text{halo}}$	N_{eject}	f_{surv}	f_{ICS}	α_{start}	α_{end}
D1	1394.6	1023	345	165	83	0	0	0.420	0.127	-1.38	-1.33
D2	1374.4	866	330	97	37	0	1	0.463	0.085	-1.38	-1.33
D3	1431.1	906	257	199	187	0	0	0.290	0.125	-1.39	-1.32
D4	1163.2	754	211	152	120	0	0	0.359	0.117	-1.33	-1.26
D5	1239.5	788	283	167	197	0	0	0.179	0.167	-1.33	-1.21
D6	1158.8	527	131	59	53	0	1	0.537	0.065	-1.34	-1.30
D7	1300.7	663	236	85	73	0	1	0.404	0.151	-1.37	-1.31
D8	1298.4	773	296	113	116	0	0	0.321	0.120	-1.36	-1.33
D9	1299.5	652	256	95	63	0	1	0.364	0.141	-1.39	-1.33
D10	1169.4	589	193	76	67	0	1	0.428	0.106	-1.37	-1.32
D11	1145.8	741	282	143	79	0	1	0.318	0.124	-1.38	-1.25
D12	1227.5	732	235	57	22	0	9	0.559	0.075	-1.39	-1.35
D13	1334.2	952	330	166	70	0	0	0.406	0.151	-1.35	-1.31
D14	1286.0	844	283	184	115	0	1	0.309	0.203	-1.34	-1.24
D15	1470.8	888	298	115	56	0	0	0.472	0.140	-1.36	-1.33
D16	1454.4	966	288	170	125	0	0	0.396	0.086	-1.34	-1.30

TABLE 6
SIMULATIONS FOR SERIES E

Run	$M_{\text{total}}[10^{11} M_{\odot}]$	N_{total}	N_{merge}	$N_{\text{tides}}^{\text{gal}}$	N_{accr}	$N_{\text{tides}}^{\text{halo}}$	N_{eject}	f_{surv}	f_{ICS}	α_{start}	α_{end}
E1	1065.4	1023	406	159	24	8	1	0.415	0.297	-1.38	-1.31
E2	1034.0	866	326	104	7	6	2	0.486	0.168	-1.38	-1.31
E3	1051.3	906	405	213	19	14	0	0.282	0.446	-1.38	-1.27
E4	799.4	754	250	177	35	7	0	0.378	0.391	-1.34	-1.25
E5	868.7	788	394	201	42	12	0	0.176	0.492	-1.32	-1.22
E6	795.8	527	154	67	7	6	1	0.554	0.303	-1.34	-1.29
E7	947.7	663	276	97	9	3	1	0.418	0.376	-1.37	-1.31
E8	941.0	773	395	121	11	8	0	0.307	0.348	-1.37	-1.28
E9	934.5	652	263	109	10	6	1	0.403	0.325	-1.39	-1.34
E10	807.5	589	210	98	11	5	1	0.325	0.448	-1.38	-1.35
E11	760.7	741	349	142	9	8	1	0.313	0.283	-1.48	-1.23
E12	946.4	732	227	57	4	2	28	0.566	0.149	-1.39	-1.35
E13	953.4	952	344	180	14	11	0	0.423	0.349	-1.35	-1.29
E14	950.5	844	325	197	23	6	1	0.346	0.395	-1.33	-1.29
E15	1145.5	888	320	118	13	5	0	0.486	0.339	-1.36	-1.29
E16	1125.4	966	439	146	10	10	1	0.373	0.393	-1.34	-1.26

most notable feature is that some galaxies are destroyed by the tidal field of the background halo, something that never happened with Virgo-like clusters. In order to explain such a behavior we note that tidal disruption by the cluster halo generally occurs with galaxies at a distance $r \lesssim 1$ Mpc from the cluster center. Our simulated Perseus-like cluster halo mass profile rises more steeply than the Virgo-like cluster up to ~ 1.7 Mpc, making Perseus more massive in the inner regions. So a galaxy at a smaller distance, precisely at $r \lesssim 1.7$ Mpc, from the cluster center feels a larger tidal field from a more massive halo, and is more prone to be disrupted in the Perseus-like cluster.

The numbers of other galaxy outcomes are comparable for Perseus-like and Virgo-like clusters, with mergers dominating over tides. The mean f_{ICS} for series E is

$$f_{\text{ICS}} = 0.344 \pm 0.093. \quad (33)$$

This f_{ICS} is somewhat larger than the Virgo-like cluster mean (series C). This can be attributed to the non-zero tidal disruption by the cluster halo, resulting here in a finite contribution to the ICS mass fraction.

Table 7 shows the results for series F, i.e., simulations of a Perseus-like cluster with a cD galaxy at the center. Here few galaxies are destroyed by the tidal field of the cluster halo, yet the number is smaller than in series E. It appears, then that the presence of a cD galaxy reduces the number of tidal disruptions by the background halo, since galaxies that would be destroyed by the tidal field of the central parts of the halo are being destroyed by the cD galaxy instead.

Comparing the results for series D and series F (Virgo-like and Perseus-like clusters with a cD galaxy,) the numbers-merger, galaxy-tide and accretion are similar. Series F continues the trend of increased accretions when a cD galaxy is introduced. Also series F has a smaller fraction of mass going to ICS. The mean f_{ICS} for series F is

$$f_{\text{ICS}} = 0.128 \pm 0.031. \quad (34)$$

This f_{ICS} is very similar to that of the relevant Virgo-like cluster mean (series D). This implies that in the presence of a cD galaxy, the ICS mass fraction is not so sensitive to the parameters of the β -model density profile.

4.6. Series G, H, & I: NFW Profile

We now consider a background halo described by a NFW profile [see §2.3, eq. (4)], with a scale radius $r_s = 200$ kpc, and a concentration parameter $c = 5$. These values are adopted from observational studies of galaxy clusters (Arabadjis, Bautz, & Garmire 2002; Pratt & Arnaud 2005; Maughan et al. 2007) where the authors found the best fitting NFW model parameters for cluster mass profiles.

We do not necessarily expect the flattening of the Schechter mass function to be the same for the NFW profile halo and the β -profile halo. So at first we performed a series with $\alpha = -1.28$ (see Table 1), and called it series G. The results are listed in Table 8.

To contrast a NFW-model cluster with a β -model cluster, Series G should be compared with Series B, since these are with $\alpha = -1.28$, include galaxy harassment, and no cD galaxy. The most striking feature is the large number of galaxies destroyed by the tidal field of the

NFW cluster halo. This halo tidal disruption was nil (in the Virgo-like cluster) to a handful (in the Perseus-like cluster) for the β -model background halo. With the NFW profile, the number of halo tides is comparable to the galaxy tides, even exceeding the latter in runs G5 and G6.

The reason for such a behavior is that the NFW halo mass profile rises much more steeply than the β -model mass profile of a Virgo-like cluster up to a distance $r \sim 1.9$ Mpc. So the NFW halo is significantly more massive (by factors as high as 4 – 5) than the β -model halo at distances $r \lesssim 1$ Mpc, where halo tides are dominant (as discussed in §4.5). Consequently galaxies near the cluster center experience a larger tidal field and are more likely to be tidally disrupted.

This larger number of halo tides alters several results in our simulated NFW model cluster as compared to the β -model. The mergers exceed the galaxy tides, usually by factors 1.3-1.8 (except runs G6 and G10, where the factors are 3 and 2.5). But when tides by galaxy and cluster halo are added together, they become comparable to or even exceed the number of mergers. The accretions are always small in number, and when added to mergers do not have much effect on the above.

The mean f_{ICS} for series G is

$$f_{\text{ICS}} = 0.436 \pm 0.117. \quad (35)$$

This is significantly larger than the ICS mass fraction obtained with the β -model clusters. The reason is again the numerous halo tides. Some massive galaxies are being destroyed by the tidal field of the NFW halo, when they come near the cluster center, and this is contributing a large mass fraction to the ICS.

In this series G, we obtained the average values of α as

$$\alpha_{\text{start}} = -1.285 \pm 0.022, \quad (36)$$

$$\alpha_{\text{end}} = -1.258 \pm 0.034. \quad (37)$$

Also combining the set of galaxies of all the 10 runs in series G, we obtained the best fit Schechter exponent for the surviving galaxy distribution at $z = 0$ as $\alpha = -1.25$. Analogous to our approach for the β -model in §4.3, we note that $|\alpha|$ decreases by ~ 0.03 between $z = 1$ and $z = 0$. So we performed a new series of simulations, series H, using $\alpha_{\text{start}} = -1.31$, expecting that this will evolve to $\alpha \sim -1.28$ at $z = 0$. This series includes galaxy harassment but no cD galaxy. The results for series H are shown in Table 9.

Series H continues the trends of series G pertaining to a NFW profile. There are a large number of halo tides that dominate the mass fraction, and result in a high value of f_{ICS} . The combined numbers of tidal disruptions (by galaxy and halo) are comparable to or exceed the numbers of mergers. The mean f_{ICS} for series H is

$$f_{\text{ICS}} = 0.471 \pm 0.129. \quad (38)$$

In this series H, we obtained the average values of α as

$$\alpha_{\text{start}} = -1.310 \pm 0.020, \quad (39)$$

$$\alpha_{\text{end}} = -1.288 \pm 0.036. \quad (40)$$

We then performed a series of simulations by putting

TABLE 7
SIMULATIONS FOR SERIES F

Run	$M_{\text{total}}[10^{11}M_{\odot}]$	N_{total}	N_{merge}	$N_{\text{tides}}^{\text{gal}}$	N_{accr}	$N_{\text{tides}}^{\text{halo}}$	N_{eject}	f_{surv}	f_{ICS}	α_{start}	α_{end}
F1	1394.6	1023	386	153	88	4	1	0.382	0.138	-1.38	-1.28
F2	1374.4	866	304	96	47	1	2	0.480	0.106	-1.38	-1.33
F3	1431.1	906	277	183	196	1	0	0.275	0.144	-1.39	-1.25
F4	1163.2	754	211	180	109	0	0	0.337	0.126	-1.33	-1.27
F5	1239.5	788	288	166	199	0	0	0.171	0.158	-1.33	-1.21
F6	1158.8	527	141	60	55	1	1	0.510	0.092	-1.34	-1.29
F7	1300.7	663	253	81	70	1	1	0.388	0.113	-1.37	-1.28
F8	1298.4	773	295	124	108	2	0	0.316	0.134	-1.36	-1.29
F9	1299.5	652	226	93	61	2	1	0.413	0.153	-1.39	-1.38
F10	1169.4	589	182	83	72	0	1	0.426	0.133	-1.37	-1.33
F11	1145.8	741	269	148	76	1	1	0.332	0.154	-1.38	-1.29
F12	1227.5	732	194	58	26	0	31	0.578	0.067	-1.39	-1.36
F13	1334.1	952	322	175	85	1	0	0.388	0.121	-1.35	-1.29
F14	1286.0	844	272	180	107	0	1	0.336	0.197	-1.34	-1.30
F15	1470.8	888	306	103	54	1	0	0.478	0.108	-1.36	-1.31
F16	1454.4	966	314	155	135	2	1	0.372	0.097	-1.34	-1.29

TABLE 8
SIMULATIONS FOR SERIES G

Run	$M_{\text{total}}[10^{11}M_{\odot}]$	N_{total}	N_{merge}	$N_{\text{tides}}^{\text{gal}}$	N_{accr}	$N_{\text{tides}}^{\text{halo}}$	N_{eject}	f_{surv}	f_{ICS}	α_{start}	α_{end}
G1	721.9	372	72	55	6	47	1	0.513	0.486	-1.27	-1.26
G2	1034.3	637	129	80	4	63	7	0.556	0.405	-1.29	-1.26
G3	821.1	530	127	89	5	73	1	0.443	0.587	-1.31	-1.29
G4	992.3	457	113	61	9	44	1	0.501	0.211	-1.28	-1.26
G5	899.7	618	94	56	7	64	8	0.629	0.443	-1.29	-1.28
G6	947.1	452	95	31	2	34	17	0.604	0.263	-1.31	-1.32
G7	865.2	542	170	91	7	77	1	0.362	0.543	-1.31	-1.25
G8	1011.6	725	169	101	7	71	1	0.519	0.502	-1.24	-1.20
G9	1100.6	726	214	144	17	103	1	0.340	0.467	-1.27	-1.23
G10	1174.4	619	190	76	2	57	6	0.465	0.458	-1.28	-1.23

TABLE 9
SIMULATIONS FOR SERIES H

Run	$M_{\text{total}}[10^{11}M_{\odot}]$	N_{total}	N_{merge}	$N_{\text{tides}}^{\text{gal}}$	N_{accr}	$N_{\text{tides}}^{\text{halo}}$	N_{eject}	f_{surv}	f_{ICS}	α_{start}	α_{end}
H1	894.3	755	171	152	5	122	0	0.404	0.620	-1.33	-1.33
H2	866.2	556	195	68	5	92	1	0.351	0.563	-1.28	-1.24
H3	955.0	621	161	84	2	67	1	0.493	0.396	-1.33	-1.35
H4	758.6	588	153	113	7	109	1	0.349	0.702	-1.30	-1.30
H5	1103.6	997	197	132	5	68	22	0.575	0.375	-1.30	-1.26
H6	1008.7	774	266	162	10	148	0	0.243	0.682	-1.29	-1.24
H7	1027.4	639	101	40	4	47	28	0.656	0.316	-1.32	-1.30
H8	833.8	601	126	75	5	70	7	0.529	0.496	-1.29	-1.28
H9	740.3	494	109	53	9	54	4	0.536	0.398	-1.30	-1.28
H10	952.9	744	159	96	13	92	1	0.515	0.451	-1.35	-1.32
H11	779.4	519	113	54	9	59	2	0.543	0.375	-1.31	-1.25
H12	993.6	741	163	86	3	57	10	0.570	0.306	-1.33	-1.29
H13	931.8	534	131	60	5	62	2	0.513	0.412	-1.31	-1.33
H14	1012.8	748	202	117	8	95	1	0.434	0.508	-1.30	-1.26

a cD galaxy at the center of the NFW cluster halo, and called it series I. The results are shown in Table 10. Here, the numbers of tides by the cluster halo and by other galaxies are comparable; when added the total occurrence of tides compares to or exceeds that of mergers. Comparing series H and series I (NFW-type clusters respectively without and with a cD galaxy,) there are more accretions when a cD galaxy is introduced (similar to series D and F). The trend seen before with the Perseus-like clusters (between series E and F), that the number of

tidal disruptions by the background halo reduces in the presence of a cD galaxy, is almost absent in the NFW-type clusters. Galaxies approaching the cluster center get destroyed by the tidal field of the halo before the cD galaxy can have any effect.

The galactic mass fractions dispersed into the ICM are neither too high, nor too low. We suspect this is the combined effect of putting a cD galaxy in a NFW type cluster. There is a tendency of the ICS mass fraction to be high in a NFW model cluster, and a cD galaxy

TABLE 10
SIMULATIONS FOR SERIES I

Run	$M_{\text{total}}[10^{11}M_{\odot}]$	N_{total}	N_{merge}	$N_{\text{tides}}^{\text{gal}}$	N_{accr}	$N_{\text{tides}}^{\text{halo}}$	N_{eject}	f_{surv}	f_{ICS}	α_{start}	α_{end}
I1	1189.1	495	114	53	26	75	1	0.457	0.322	-1.34	-1.31
I2	1255.5	705	183	100	16	87	0	0.452	0.326	-1.34	-1.32
I3	1189.9	643	152	127	35	119	0	0.327	0.391	-1.29	-1.31
I4	1153.5	548	108	78	8	66	1	0.524	0.255	-1.32	-1.30
I5	1309.4	821	228	139	19	87	1	0.423	0.341	-1.33	-1.31
I6	1330.8	596	105	56	2	54	9	0.621	0.265	-1.31	-1.30
I7	1315.8	775	215	126	37	105	0	0.377	0.299	-1.33	-1.31
I8	1188.1	691	118	91	12	71	1	0.576	0.248	-1.36	-1.35
I9	1236.6	574	103	73	12	56	1	0.573	0.295	-1.32	-1.30
I10	1093.4	634	96	96	8	64	1	0.582	0.274	-1.31	-1.29

TABLE 11
SERIES FOR PARAMETER VARIATIONS
OF β -MODEL HALO DENSITY PROFILE

Series	β	ρ_0 [g cm^{-3}]	r_c [kpc]
Bb1	0.3	1.0×10^{-26}	50
Bb2	0.4	1.0×10^{-26}	50
Bb3	0.5	1.0×10^{-26}	50
Bb4	0.6	1.0×10^{-26}	50
Bb5	0.8	1.0×10^{-26}	50
Bb6	1.0	1.0×10^{-26}	50
Br1	0.5	1.0×10^{-26}	10
Br2	0.5	1.0×10^{-26}	100
Br3	0.5	1.0×10^{-26}	200
Br4	0.5	1.0×10^{-26}	300
Br5	0.5	1.0×10^{-26}	400
Br6	0.5	1.0×10^{-26}	500

tends to reduce the mass fraction imparted to the ICM. These two opposing trends cause the f_{ICS} values to be moderate in series I. Here the mean f_{ICS} is

$$f_{\text{ICS}} = 0.302 \pm 0.044. \quad (41)$$

5. DEPENDENCE ON PARAMETERS OF CLUSTER HALO DENSITY PROFILE

5.1. β -Model

We investigated the dependence of the galaxy outcomes and the ICS mass fraction on the parameters governing the cluster halo density profile. For the β -model halo density (see §2.3), we found that the typical values of the relevant parameters cover the range $\beta = 0.3 - 1$, the core radius $r_c = 3 - 600$ kpc, the core number density $n_0 = (0.1 - 100) \times 10^{-3} \text{ cm}^{-3}$, corresponding to a physical density $\rho_0 = (0.017 - 17) \times 10^{-26} \text{ g cm}^{-3}$. We obtained these values from several observational studies, Lea et al. (1973); Abramopoulos & Ku (1983); Jones & Forman (1984); Waxman & Miralda-Escude (1995); Makino, Sasaki, & Suto (1998); Girardi et al. (1998); Ettori (2000); Xue & Wu (2000); Biviano & Girardi (2003); Piffaretti & Kaastra (2006); Maughan et al. (2007).

We performed a series of simulations, as shown in Table 11, doing 5 runs in each series, for a total of 60 simulations. These were done using a Schechter mass distribution exponent $\alpha = -1.36$ (see §4.3), and including galaxy harassment, but not including a cD galaxy.

In series Bb1 - Bb6 (Table 11), we explored values of β between 0.3 - 1.0, with fixed $r_c = 50$ kpc, and

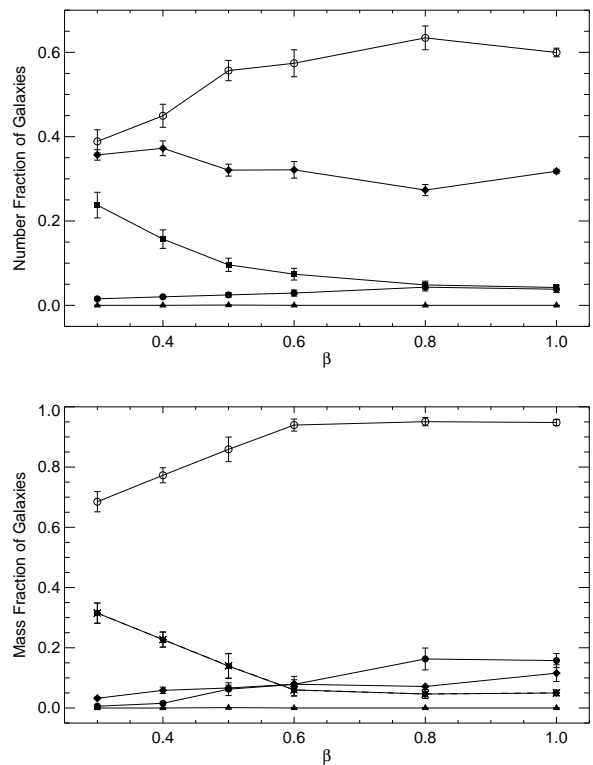


FIG. 5.— Number fractions (upper panel) and mass fractions (lower panel) of galaxies having different outcomes as a function of parameter β of β -model halo density profile (see §5.1). The symbols show the mean galaxy fractions and the error bars are the errors on the mean values. The common plotting symbols for both panels are: *diamond* - merger, *square* - tidal destruction by a massive galaxy with fragments going to ICM, *filled circle* - accretion after galaxy tidal disruption, *triangle* - tidal destruction by the halo, *open circle* - survival up to the present. In addition, the lower panel shows the galactic mass fraction that ends up in the ICM, f_{ICS} , with *asterisk* plotting symbol, and joined by a *dashed* line. On this panel, the asterisks and the dashed line are indistinguishable from the squares and the line connecting them.

$\rho_0 = 1.0 \times 10^{-26} \text{ g cm}^{-3}$ (which corresponds to a particle number density $n_0 = 6.0 \times 10^{-3} \text{ cm}^{-3}$). We found the arithmetic means and the uncertainties on the arithmetic means ($= \sigma/\sqrt{5}$) of the galaxy fraction results from the 5 runs in each series. The resulting average fractions of each outcome are plotted in Figure 5 as a function of β , with the galaxy number fractions in the upper panel, and the mass fractions in the lower panel. Occurrences

of ejection out of the cluster (§2.4.5) are not shown, since they are either zero or negligibly small compared to the other outcomes. As a note, for a certain value of β , the number fractions of the different galaxy outcomes will add up to 1. But the added mass fraction of all the outcomes will be > 1 , because there is a double counting of the mass of galaxies merging and accreting. The mass fraction of galaxies surviving, the mass imparted to the ICM by tidal disruptions (due to other galaxies and cluster halo), and that ejected, will add up to 1.

From Figure 5 we see that an increase in β causes a decline of galaxy interactions, leading to survival of more and more galaxies up to $z = 0$. The numbers of mergers dominate over galaxy tides by a factor of 2 or more. But only the low-mass galaxies merge, making the merged mass fraction significantly smaller than the tidal destruction mass fraction when $\beta < 0.6$. With increase of β from 0.3 to 0.6, destruction by galaxy tides (with the fragments imparted to the ICM) decline dramatically, mergers have a slight decrease in number but increase in mass (implying that more massive galaxies are merging), accretions increase but always remaining below mergers and galaxy tides. In between $\beta = 0.6 - 1.0$ there is not much change in the resulting galaxy fractions, the trends continue slowly as β reaches 1. A noteworthy result is that at $\beta > 0.6$ galaxy accretion dominates the mass fraction compared to the other outcomes. Tidal disruption by the halo and ejection out of the halo are either zero, or negligibly small in number and mass, for all β .

The mass fraction f_{ICS} of galaxies imparted to the ICM by tidal disruptions is shown in the lower panel of Figure 5 with *asterisk* symbols joined by a *dashed* line. This curve is not distinguishable since, for this set of simulations, the ICS mass comes only from the dwarf galaxies destroyed by the tides of more massive galaxies. So f_{ICS} coincides with the *solid* line showing the galaxy tides fraction, with the *asterisk* symbols coinciding with the *squares*. As β rises between 0.3 – 0.6, the ICS mass fraction decreases from ~ 0.3 to ~ 0.1 . After that f_{ICS} is essentially constant at ~ 0.1 when $\beta > 0.6$.

Next, we explore variations of the core radius r_c in between 10 – 500 kpc, in series Br1 – Br6 (Table 11). Here $\beta = 0.5$, and $\rho_0 = 1.0 \times 10^{-26} \text{ g cm}^{-3}$ are kept fixed. We calculated and analyzed the results in a way analogous to that done for series Bb1 – Bb6. The means and the errors on the means (from the 5 random runs in each series) of the resulting galaxy fractions with a specific outcome are plotted in Figure 6 as a function of r_c .

From Figure 6, the following trends can be inferred about the dependence of the results on the core radius. As r_c rises, a decreasing number of galaxies survive up to $z = 0$, leading to an increase in the mass incorporated to the ICM. When $r_c > 50$ kpc, the mass fraction is increasingly dominated by galaxies getting destroyed by other galaxy tides with the fragments being dispersed into the ICM. Mergers outnumber galaxy tides when r_c is small, become comparable to tides at $r_c \sim 350$ kpc, and at large- r_c tides dominate. But only the low-mass galaxies merge (similar to series Bb1 – Bb6), causing the merged mass fraction to be significantly smaller than that tidally destroyed. As r_c increases, galaxy tides increase substantially by number and mass, mergers remain almost con-

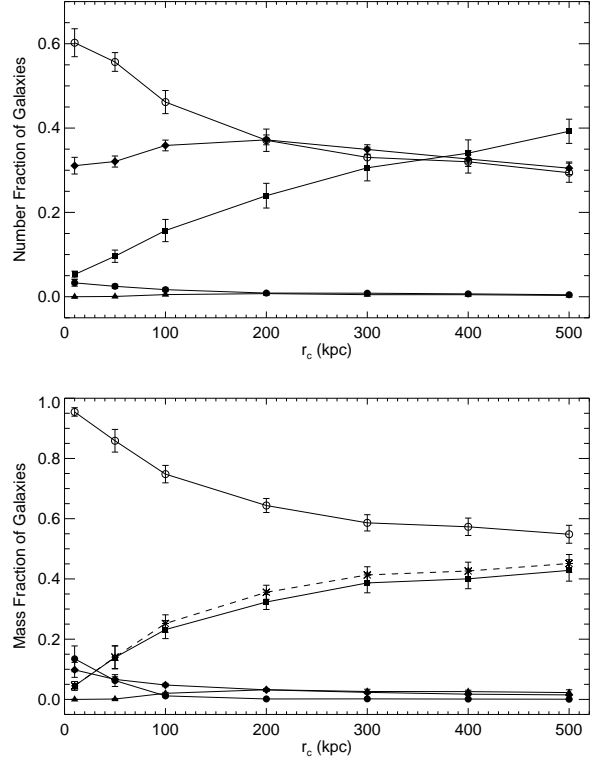


FIG. 6.— Number fractions (upper panel) and mass fractions (lower panel) of galaxies having different outcomes, and mass fraction imparted to the ICM, f_{ICS} (lower panel), as a function of the core radius, r_c , of β -model halo density profile. The plotting symbols are same as in Figure 5. See §5.1 for discussions.

stant with a small reduction at large- r_c , and accretions (which have a small contribution) decline. There are a few cases of tidal destruction by the cluster halo when $r_c \geq 100$ kpc, which has a few % contribution by number and mass. The number of occurrences of ejection from the halo is always negligibly small in number and mass.

The lower panel of Figure 6 shows f_{ICS} , the mass fraction transferred to the ICM by destruction due to tides, as *asterisk* symbols joined by a *dashed* line. f_{ICS} is largely dominated by the galactic mass destroyed by the tides of more massive galaxies (*squares* joined by *solid* lines). There is a small contribution coming from tidal disruptions by the cluster halo, which gets added to the resultant f_{ICS} . With increase of r_c between 10 – 500 kpc, the ICS mass fraction rises from ~ 0.05 to ~ 0.45 .

5.2. NFW Model

We explored the dependence of the galaxy outcomes and the ICS mass fraction on the parameters governing the NFW model cluster halo density profile (see §2.3). Typical ranges of the profile parameters cover values of the scale radius $r_s = 100 - 500$ kpc, and the concentration parameter $c = 3 - 6$. We obtained these values from several observational works, Carlberg et al. (1997); van der Marel et al. (2000); Arabadjis, Bautz, & Garmire (2002); Pratt & Arnaud (2002); Biviano & Girardi (2003); Pointecouteau, Arnaud & Pratt (2005); Pratt & Arnaud (2005); Maughan et al. (2007).

Table 12 shows the series of simulations we performed,

TABLE 12
SERIES FOR PARAMETER
VARIATIONS OF NFW
MODEL HALO DENSITY
PROFILE

Series	c	r_s [kpc]
Nr1	4.5	10
Nr2	4.5	50
Nr3	4.5	100
Nr4	4.5	200
Nr5	4.5	300
Nc1	4	100
Nc2	6	100

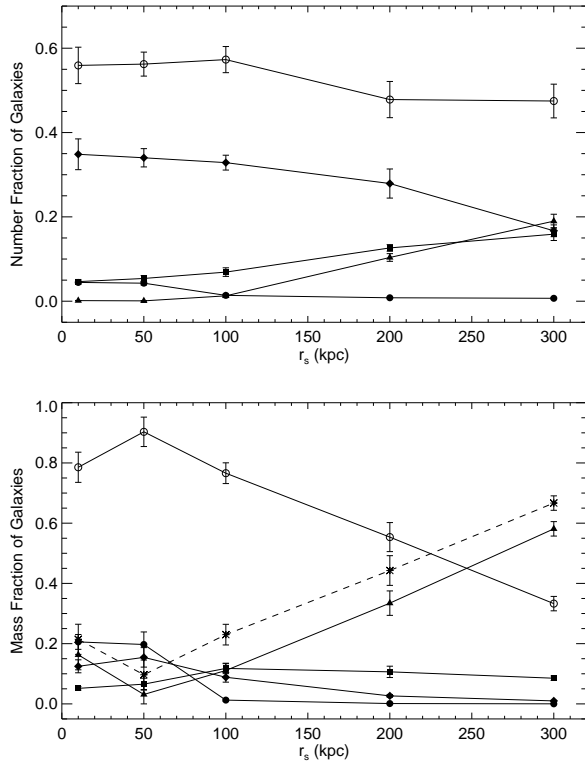


FIG. 7.— Number fractions (upper panel) and mass fractions (lower panel) of galaxies having different outcomes, and mass fraction imparted to the ICM, f_{ICS} (lower panel), as a function of the scale radius, r_s , of NFW-model halo density profile. The plotting symbols are same as in Figure 5. See §5.2 for discussions.

doing 5 random runs in each series, for a total of 35 simulations. For this set, we used a Schechter mass distribution exponent $\alpha = -1.31$ (see reasoning in §4.6), included galaxy harassment, but did not include a cD galaxy.

In series Nr1 – Nr5 (Table 12), we investigate five different values of the scale radius r_s within 10 – 300 kpc, keeping the concentration fixed at $c = 4.5$. We present the results in a manner analogous to that done for series Bb1 – Bb6 and Br1 – Br6 in §5.1. Figure 7 shows the means and the errors on the means (from the 5 random runs in each series) of the resulting galaxy fractions with a specific outcome as a function of r_s .

Some general trends are clear from Figure 7 about the

dependence of the results on the scale radius. With increase of r_s , a smaller number of galaxies survive up to the present, causing greater mass transferred to the ICM. The most noteworthy feature of these NFW simulations is that a large galactic mass fraction is tidally destroyed by the cluster halo. In fact when $r_s \geq 100$ kpc, the mass fraction is increasingly dominated by galaxies getting destroyed by tidal field of the halo, with the fraction reaching as high as ~ 0.6 when $r_s = 300$ kpc. These disrupted galaxy fragments are unconditionally dispersed into the ICM, which increases the ICS mass fraction substantially.

The number of mergers is higher than that of tides by galaxy and halo when r_s is small; but these numbers of mergers, galaxy tides and halo tides become comparable at $r_s \sim 300$ kpc. At the same time, the galaxies merging have smaller masses (similar to the results in §5.1), making the merged mass fraction comparable to that tidally destroyed by galaxies, both of which are hugely outweighed by halo tides. As r_s increases, tidal disruption by the halo rise significantly, galaxy tides increase slightly in number but decrease in mass (implying lower mass galaxies are tidally destroyed by other galaxies), and mergers decline. Similar to the results in §5.1, ejection out of the cluster is always negligibly small in number and mass.

The galactic mass fraction imparted to the ICM by tidal destructions is shown in the lower panel of Figure 7. As discussed in previous paragraphs, here f_{ICS} is largely dominated by the galactic mass destroyed by the tides of the cluster halo (*triangles* joined by *solid* lines). Tidal disruption by other galaxies have a small contribution to f_{ICS} . As r_s rises between 10 – 300 kpc, the ICS mass fraction grows from ~ 0.1 to ~ 0.65 .

Finally, we performed 2 series of simulations, Nc1 and Nc2 (Table 12), varying the concentration parameter to $c = 4$ and 6, with a fixed value of the scale radius $r_s = 100$ kpc. We found that the mergers continue to outnumber the tides. The average values of the ICS mass fractions are, $f_{\text{ICS}} = 0.196$ with $c = 4$, and $f_{\text{ICS}} = 0.278$ with $c = 6$.

6. DISCUSSION

6.1. Mergers vs. Tides

To quantify the relative importance of destruction by tides and by mergers, we calculated, for each run, the following fractional numbers:

$$f_{\text{destroyed}}^{\text{mergers}} = \frac{N_{\text{merge}} + N_{\text{accr}}}{N_{\text{destroyed}}}, \quad (42)$$

$$f_{\text{destroyed}}^{\text{tides}} = \frac{N_{\text{tides}}^{\text{gal}} + N_{\text{tides}}^{\text{halo}}}{N_{\text{destroyed}}}, \quad (43)$$

where $N_{\text{destroyed}} = N_{\text{merge}} + N_{\text{tides}}^{\text{gal}} + N_{\text{accr}} + N_{\text{tides}}^{\text{halo}}$. We then averaged the fractions over all the runs in each series of the simulations. The results for the set of series in Table 1 are shown in Figure 8. The destruction by mergers clearly dominates over destruction by tides for the β model, while they are of comparable importance for the NFW model.

Figure 9 gives the destruction fraction results for the set of series in Tables 11 and 12. For greater values of the index β of the β -model density (series Bb1–Bb6, Table 11), mergers rise and tides decline, causing mergers

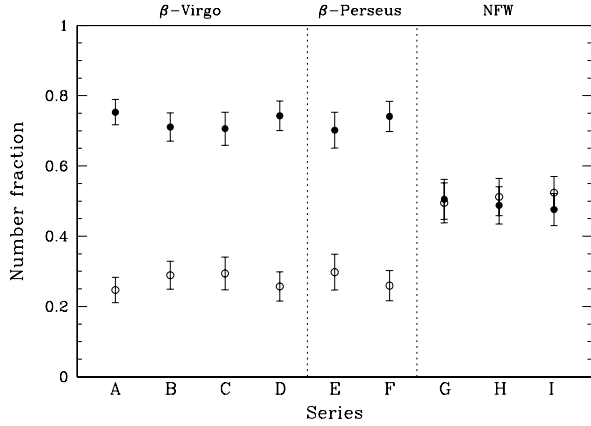


FIG. 8.— Fractional number of galaxies destroyed by mergers, $f_{\text{destroyed}}^{\text{mergers}}$ (filled circles), and by tides, $f_{\text{destroyed}}^{\text{tides}}$ (open circles), averaged over all runs within each series of Table 1. Error bars show the standard deviation.

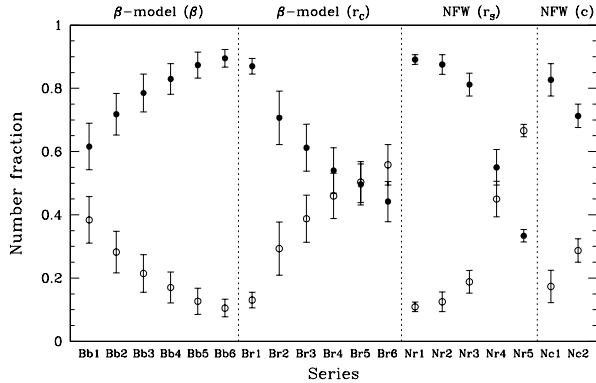


FIG. 9.— Fractional number of galaxies destroyed by mergers, $f_{\text{destroyed}}^{\text{mergers}}$ (filled circles), and by tides, $f_{\text{destroyed}}^{\text{tides}}$ (open circles), averaged over all runs within each series of Tables 11 and 12. Error bars show the standard deviation.

to increasingly dominate over tides. The trend is opposite for increasing core radius r_c of the β -model (series Br1–Br6, Table 11), and for increasing scale radius r_s of the NFW model (series Nr1–Nr5, Table 12); here mergers reduce and tides grow, such that finally (at $r_c \geq 400$ kpc, and $r_s \geq 300$ kpc) tides outnumber mergers. Destruction by mergers well dominates that by tides in series Nc1 and Nc2 (Table 12).

6.2. Intracluster Stars

Several mechanisms can contribute to removing stars from individual galaxies and putting them in the intracluster space. The efficiency and relative importance of these processes is expected to vary according to the location inside a cluster and during its evolution. If ram-pressure stripping or harassment are dominant mechanisms to produce IC stars, then the ICL fraction should increase with the mass of a cluster. On the other hand, if galaxy-galaxy merging is the dominant mechanism, and most of the ICL formed early on in cluster collapse, then the ICL fraction should be independent of present cluster

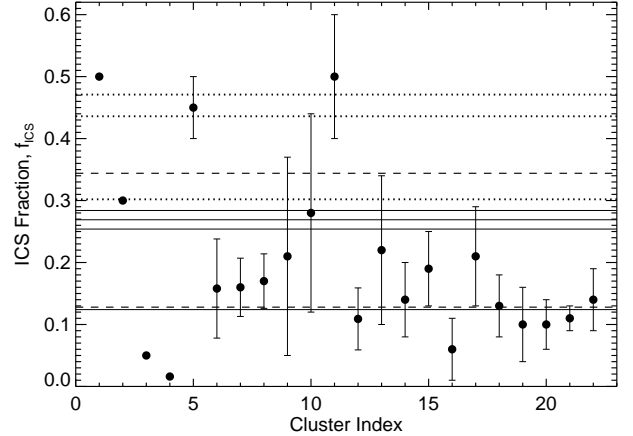


FIG. 10.— Fraction f_{ICs} of intracluster stars. The horizontal lines show the average f_{ICs} values in our simulations, from the runs of the series in Table 1 (§4), with *solid line*: Virgo-like cluster (series A–D), *dashed line*: Perseus-like cluster (series E–F), *dotted line*: NFW model cluster (series G–I). The symbols and error bars show actual measurements, as tabulated in Table 13.

mass.

The ICL fraction depends on the merger history of the cluster, presence of a cD galaxy, and the morphology of the cluster galaxies. Observations (e.g., Krick & Bernstein 2007) show that if a cD galaxy is present then the ICL profile is centrally concentrated, implying that the ICL formed by galaxy interactions at the center, or formed earlier in protoclusters and later combined at the center. The ICL fraction should evolve with redshift, as the number of galaxy interactions increase with time. Cosmological simulations indicate that the ICL fraction does increase with time as clusters evolve (Willman et al. 2004; Rudick et al. 2006).

The different formation mechanisms impart some distinct perceptible trends in the ICL. If most of the IC stars originate in initial cluster collapse, their distribution and kinematics should closely follow that of the galaxies in the cluster. If the ICL builds up slowly with time due to processes like “galaxy harassment,” “tidal stripping,” etc., then a fraction of IC stars should be located in long streams along the orbits of parent galaxies. Cosmological simulations with very high resolution is required to address these issues numerically.

There have been several observational measurements of the light (or, mass) fraction contained in the ICS with respect to the total light in a cluster. We collected some values of the ICS fraction from the literature, and list them in Table 13. In Figure 10 we show the ICS mass fraction we obtained in our simulations, plotted as horizontal lines showing the average f_{ICs} from the runs in Series A–I (Table 1, §4). For comparison, the observed f_{ICs} values (from Table 13) are shown by the symbols and error bars. We can clearly see that the ICS mass fraction in clusters from observations fall well within our simulation predictions. A few clusters have too small f_{ICs} , which are probably galaxy groups and low-mass clusters.

Our simulation results indicate that the tidal destruction of dwarf galaxies (by other galaxies and by the

TABLE 13
OBSERVED VALUES OF THE ICL MASS AS A FRACTION OF THE TOTAL CLUSTER MASS

Index	Cluster	f_{ICS} (%)	Δf_{ICS} (%)	Reference
1.	Coma	50		Bernstein et al. (1995)
2.	Abell 1689	30		Tyson & Fischer (1995)
3.	Abell 1651	< 5		Gonzalez et al. (2000)
4.	M96 (Leo) Group	< 1.6		Castro-Rodriguez et al. (2003)
5.	HCG 90	45	5	White et al. (2003)
6.	Virgo	15.8	8	Feldmeier et al. (2004b)
7.	A801	16	4.7	Feldmeier et al. (2004a)
8.	A1234	17	4.4	Feldmeier et al. (2004a)
9.	A1553	21	16	Feldmeier et al. (2004a)
10.	A1914	28	16	Feldmeier et al. (2004a)
11.	93 clusters	50	10	Lin & Mohr (2004)
12.	683 clusters	10.9	5.0	Zibetti et al. (2005)
13.	A4059	22	12	Krick & Bernstein (2007) ^a
14.	A3880	14	6	Krick & Bernstein (2007)
15.	A2734	19	6	Krick & Bernstein (2007)
16.	A2556	6	5	Krick & Bernstein (2007)
17.	A4010	21	8	Krick & Bernstein (2007)
18.	A3888	13	5	Krick & Bernstein (2007)
19.	A3984	10	6	Krick & Bernstein (2007)
20.	A141	10	4	Krick & Bernstein (2007)
21.	AC 114	11	2	Krick & Bernstein (2007)
22.	AC 118	14	5	Krick & Bernstein (2007)

^a Krick & Bernstein (2007) measured these f_{ICS} values in the r band.

cluster halo) in clusters can sufficiently explain the observed fraction of intracluster light. Supporting our conclusions, observational studies do find a significant ICL component arising from dwarf galaxies in clusters. From spectroscopic and photometric analysis, Côté et al. (2001) found that the metal poor globular cluster system associated with M87 (the cD galaxy in Virgo) is not formed in situ, but is stripped from the dwarf galaxies in Virgo. Durrell et al. (2002) observed that most of the IC red-giant branch stars in Virgo are moderately metal rich suggesting that they are tidally stripped from intermediate-luminosity galaxies, though stripping from DGs is not ruled out. McNamara et al. (1994) observed trails of IC stars and gas from the tidal disruption of a DG by a companion giant elliptical galaxy in Virgo cluster.

Results from our simulation runs (in §4 and §5) indicate that, for each cluster halo density profile, namely, β , and NFW models, f_{ICS} increases with the mass of the cluster halo. This is consistent with studies finding that more massive clusters have a larger fraction of ICL than the less massive ones (Lin & Mohr 2004; Murante et al. 2004).

6.3. Limitations of the Method

The strengths and weaknesses of the methodology used in this work both reside in our somehow original approach of using one single particle to represent each galaxy, combined with a subgrid treatment of galaxy mergers, tidal disruption, and galaxy harassment.

On the positive side, this approach has enabled us to perform a very large number of simulations (227 total), covering a fairly large parameter space, while obtaining statistically significant results. In particular, the dispersion of the results seen in Tables 2–10 justifies a posteriori the number of simulations we have performed. Doing this many simulations without resorting to subgrid physics would have been computationally prohibitive. In addi-

tion, this approach greatly facilitates the analysis and interpretation of the results. In a simulation in which a galaxy would be represented by a large numbers of particles, a dwarf galaxy could be partly destroyed by tides, with some fragments being dispersed in the ICM, other fragments accreting onto the larger galaxy, with enough of the galaxy surviving that it can still be counted as a galaxy. It would then become more difficult to quantify objectively the relative importance of mergers and tidal disruptions.

In implementing the subgrid physics, we have attempted to make the most reasonable choices possible. One free parameter is the geometric factor entering in equation (10), but for reasonable density profiles, the values of that factor do not appear to vary much. The assumption that a galaxy is considered “tidally disrupted” if 50% of its mass becomes unbound is also the most reasonable one we could make.

Our technique for generating the initial conditions is based on four key assumptions: (1) the galaxy distributions are isotropic, (2) the galaxy number density profile $\nu(r)$ follows the density profile $\rho_{\text{halo}}(r)$ of the background cluster halo, (3) the mass is segregated in the cluster, with the most massive galaxies being located in the center, and (4) the cluster is in equilibrium. So even though our prescription for generating the initial conditions contains many tunable parameters, we believe that the underlying approach is sound.

On the negative side, two particular aspects of the methodology can be considered weak. First, the treatment of galaxy harassment is highly speculative. We have assumed that some amount of orbital kinetic energy ΔE is dissipated into internal energy during an encounter between two galaxies, that this amount is related to the initial internal energies of the galaxies, and that the energy dissipated is distributed equally between the two galaxies. The dissipation of energy and its consequences during a real galactic encounter are certainly

much more complex, so the subgrid model could potentially be refined. But this would require an intensive study of high-speed encounters, with detailed numerical simulations, and such study remains to be done.

Another important limitation of our approach is that it deals with isolated clusters in equilibrium. In the real universe, clusters constantly experience mergers and accretion. We justify our approach by the fact that most clusters will experience, at some epoch, a *major merger*, during which most of the final mass of the cluster is assembled. From that point, if we can neglect the addition of mass by minor mergers and accretion, the cluster can be treated as isolated. Of course, such scenario cannot describe all clusters. In a forthcoming paper (Brito et al. 2008), we will present a study of cluster formation and evolution inside a cosmological volume containing many clusters. This will be achieved by implementing the subgrid approach described in this paper into a cosmological N-body algorithm.

7. SUMMARY AND CONCLUSION

We have designed a simple model for the evolution of galaxies in an isolated cluster, in order to compare the destruction of dwarf galaxies by mergers vs. tidal disruptions, and to predict the contribution of dwarf galaxies to the origin of intracluster stars. Our algorithm combines a direct N-body computation of gravitational interactions, along with a subgrid treatment of the other physical processes (merger, tidal disruption, accretion etc.) of the galaxies. Using this algorithm, we have performed a total of 227 numerical simulations of galaxy clusters, examining the fate of dwarf galaxies. Our results and conclusions are as follows.

(1) The destruction of dwarf galaxies by mergers dominates over destruction by tides, in most of our simulation runs with all the models (β -Virgo, β -Perseus, NFW) of cluster halo density. The two destruction mechanisms become comparable, and tides outnumber mergers, for the NFW and the β - models when their scale/core ra-

dius approach and exceed ~ 200 -300 kpc.

(2) The destruction of dwarf galaxies by the tidal field of other galaxies and by the cluster halo imparts a significant amount of galactic mass into the ICM. This is sufficient to account for the observed fraction of intracluster light in galaxy clusters. In our simulations, the ICS mass fraction, f_{ICS} , has a range 4.5% – 66.7% (with the majority of values being in between 10% – 45%), for the different parameter sets of the β and NFW models of cluster halo density we considered. We see a clear trend of increase of f_{ICS} with the mass of the cluster halo. All these are well consistent with observations and other numerical studies.

(3) In the NFW model simulated clusters, there are a large number of tidal disruptions of galaxies caused by the gravitational potential of the cluster halo, and this component dominates the mass fraction. We note that it has been our assumption that the cluster halo is stationary, and does not evolve in response to the forces exerted on it by the galaxies (§2.1). Such an assumption is probably a poor one with the NFW model clusters. We point out that this could imply a possible solution to the cusp crisis of cluster dark matter halos. The central cuspy region of the cluster dark matter halo could have inelastic encounters with the member galaxies, which could inject energy into the halo and erase the cusp.

(4) In our simulations, the presence of a cD galaxy increases occurrences of accretion, decreases tidal disruptions by the cluster halo, and reduces the ICS mass fraction. This is opposite to the trend seen from observations that f_{ICS} is higher in the presence of a cD.

This work benefited from stimulating discussions with L. Edwards and C. Robert. We thank John Kormendy for useful correspondence. All calculations were performed at the Laboratoire d’astrophysique numérique, Université Laval. We thank the Canada Research Chair program and NSERC for support.

APPENDIX

THE INTERNAL ENERGY OF GALAXIES

Since we represent galaxies as individual particles, we cannot directly compute their internal energy. We therefore need an estimate that can then be used in equation (10). We write the potential energy of a galaxy of mass M and radius R as

$$W = -\frac{\zeta GM^2}{R}, \quad (\text{A1})$$

where ζ is the *geometric factor*, which depends on the shape and density distribution of the galaxy. For a uniform-density sphere, $\zeta = 3/5$. In our simplified model, we treat galaxies as spheres, but we should certainly not assume a uniform density. Instead, any galaxy will be centrally concentrated. The value of ζ will depend on the assumed density profile, but we do not expect that dependence to be very strong if we stick with reasonable profiles. So we consider the simplest case of an isothermal sphere with a cutoff radius R . The density and mass inside r are given by

$$\rho(r) = \frac{M}{4\pi Rr^2}, \quad (\text{A2})$$

$$m(r) = \frac{Mr}{R}, \quad (\text{A3})$$

where $M \equiv m(R)$ is the total mass. The gravitational field is given by

$$\mathbf{g} = -\nabla\phi = -\frac{Gm(r)}{r^2}\hat{r} = -\frac{GM}{rR}\hat{r}. \quad (\text{A4})$$

We integrate this expression, with the boundary condition $\phi(R) = -GM/R$, to get the gravitational potential,

$$\phi = \frac{GM}{R} \left(\ln \frac{r}{R} - 1 \right). \quad (\text{A5})$$

The potential energy is given by

$$W = \frac{1}{2} \iiint \phi(r) \rho(r) d^3r = \frac{GM^2}{2R^2} \int_0^R \left(\ln \frac{r}{R} - 1 \right) dr = -\frac{GM^2}{R}. \quad (\text{A6})$$

Hence, $\zeta = 1$ for an isothermal sphere. Interestingly, this is not much different from the value of $3/5$ for a uniform sphere. This supports our claim that the sensitivity of ζ on the density profile is weak. For the kinetic energy, we assume that the galaxies are virialized. Hence, $K = -W/2$, and therefore the internal energy is given by

$$U = K + W = -\frac{GM^2}{2R}. \quad (\text{A7})$$

REFERENCES

- Abramopoulos, F., & Ku, W. H. M. 1983, *ApJ*, 271, 446
- Aguerri, J. A. L. et al. 2005, *AJ*, 129, 2585
- Allen, S. W., Schmidt, R. W. & Fabian, A. C. 2002, *MNRAS*, 334, L11
- Arabadjis, J. S., Bautz, M. W., & Garmire, G. P. 2002, *ApJ*, 572, 66
- Arnaboldi, M. et al. 2003, *AJ*, 125, 514
- Arnaboldi, M. 2004, *IAUS*, 217, 54
- Bernstein, G. M., Nichol, R. C., Tyson, J. A., Ulmer, M. P., & Wittman, D. 1995, *AJ*, 110, 1507
- Biviano, A., & Girardi, M. 2003, *ApJ*, 585, 205
- Bothun, G. D. et al. 1991, *ApJ*, 376, 404
- Brainerd, T. G., & Specian, M. A. 2003, *ApJ*, 593, L7
- Brito, W., Martel, H., & Barai, P. 2008, in preparation
- Byrd, G., & Valtonen, M. 1990, *ApJ*, 350, 89
- Carlberg, R. G. et al. 1997, *ApJ*, 485, L13
- Carrasco, E. R. et al. 2001, *AJ*, 121, 148
- Castro-Rodriguez, N., Aguerri, J. A. L., Arnaboldi, M., Gerhard, O., Freeman, K. C., Napolitano, N. R. & Capaccioli, M. 2003, *A&A*, 405, 803
- Cavaliere, A., & Fusco-Femiano, R. 1976, *A&A*, 49, 137
- Cellone, S. A., & Buzzoni, A. 2005, *MNRAS*, 356, 41
- Côté, S., Freeman, K. C., Carignan, C., & Quinn, P. J. 1997, *AJ*, 114, 1313
- Côté, S., Carignan, C., & Freeman, K. C. 2000, *AJ*, 120, 3027
- Côté, P. et al. 2001, *ApJ*, 559, 828
- De Propriis, R. et al. 2003, *MNRAS*, 342, 725
- Drinkwater, M. J. et al. 2003, *Nature*, 423, 519
- Durrell, P. R. et al. 2002, *ApJ*, 570, 119
- Ettori, S. 2000, *MNRAS*, 318, 1041
- Ettori, S. 2003, *MNRAS*, 344, L13
- Feldmeier, J. J., Mihos, J. C., Morrison, H. L., Harding, P., Kaib, N., & Dubinski, J. 2004a, *ApJ*, 609, 617
- Feldmeier, J. J., Ciardullo, R., Jacoby, G. H., & Durrell, P. R. 2004b, *ApJ*, 615, 196
- Ferguson, H. C., & Sandage, A. 1991, *AJ*, 101, 765
- Ferguson, H. C., Tanvir, N. R., & von Hippel, T. 1998, *Nature*, 391, 461
- Gal-Yam, A. et al. 2003, *AJ*, 125, 1087
- Gerhard, O. et al. 2005, *ApJ*, 621, L93
- Girardi, M., Giuricin, G., Mardirosian, F., Mezzetti, M., & Boschin, W. 1998, *ApJ*, 505, 74
- Gnedin, O. Y. 2003, *ApJ*, 589, 752
- Gonzalez, A. H., Zabludoff, A. I., Zaritsky, D. & Dalcanton, J. J. 2000, *ApJ*, 536, 561
- Gonzalez, A. H., Zabludoff, A. I., & Zaritsky, D. 2005, *ApJ*, 618, 195
- Gonzalez, A. H., Zaritsky, D., & Zabludoff, A. I. 2007, preprint (arXiv:0705.1726)
- Grebel, E. K. 2001, *ASPC*, 239, 280
- Gregg, M. D., & West, M. J. 1998, *Nature*, 396, 549
- Hilker, M., Infante, L., & Richtler, T. 1999, *A&AS*, 138, 55
- Hill, J. M., & Oegerle, W. R. 1998, *AJ*, 116, 1529
- Impey, C. et al. 1988, *ApJ*, 330, 634
- Jones, C., & Forman, W. 1984, *ApJ*, 276, 38
- Jordan, A., Côté, P., West, M. J., Marzke, R. O., Minniti, D., & Rejkuba, M. 2004, *AJ*, 127, 24
- Karachentseva, V. E., Karachentsev, I. D., & Boergen, F. 1985, *A&AS*, 60, 213
- Karachentsev, I. D., Karachentseva, V. E., Huchtmeier, W. K., & Makarov, D. I. 2004, *AJ*, 127, 2031
- Kauffmann, G., White, S. D. M., & Guiderdoni, B. 1993, *MNRAS*, 264, 201
- King, I. 1962, *AJ*, 67, 471
- Krick, J. E., Bernstein, R. A., & Pimblet, K. A. 2006, *AJ*, 131, 168
- Krick, J. E., & Bernstein, R. A. 2007, *AJ*, 134, 466
- Lea, S. M., Silk, J., Kellogg, E., & Murray, S. 1973, *ApJ*, 184, L105
- Lee, H. et al. 2003, *AJ*, 125, 2975
- Lewis, I. et al. 2002, *MNRAS*, 334, 673L
- Lin, Y.-T., & Mohr, J. J. 2004, *ApJ*, 617, 879
- Makino, N., Sasaki, S., & Suto, Y. 1998, *ApJ*, 497, 555
- Martel, H. 1991, *ApJ*, 377, 7
- Mateo, M. L. 1998, *ARA&A*, 36, 435
- Maughan, B. J., Jones, C., Jones, L. R., & Van Speybroeck, L. 2007, *ApJ*, 659, 1125
- Mayer, L. et al. 2001, *ApJ*, 547, L123
- McNamara, B. R. et al. 1994, *AJ*, 108, 844
- Merritt, D. 1984, *ApJ*, 276, 26
- Mieske, S., Hilker, M., Jordan, A., Infante, L. & Kissler-Patig, M. 2007, preprint, arXiv:0706.2724
- Mihos, J. C. 2004, in *Clusters of Galaxies: Probes of Cosmological Structure and Galaxy Evolution*, ed. J. S. Mulchaey, A. Dressler & A. Oemler (Cambridge: Cambridge Univ. Press), 277
- Mihos, J. C., Harding, P., Feldmeier, J., & Morrison, H. 2005, *ApJ*, 631, L41
- Miller, G. E. 1983, *ApJ*, 268, 495
- Moore, B., Katz, N., Lake, G., Dressler, A., & Oemler, A. 1996, *Nature*, 379, 613
- Mori, M., & Burkert, A. 2000, *ApJ*, 538, 559
- Murante, G. et al. 2004, *ApJ*, 607, L83
- Napolitano, N. R. et al. 2003, *ApJ*, 594, 172
- Navarro, J. F., Frenk, C. S., & White, S. D. M. 1997, *ApJ*, 490, 493
- Oegerle, W. R., & Hill, J. M. 2001, *AJ*, 122, 2858
- Phillipps, S. et al. 1998, *ApJ*, 493, L59
- Piffaretti, R., & Kaastra, J. S. 2006, *A&A*, 453, 423
- Pointecouteau, E., Arnaud, M. & Pratt, G. W. 2005, *A&A*, 435, 1
- Pratt, G. W. & Arnaud, M. 2002, *A&A*, 394, 375
- Pratt, G. W., & Arnaud, M. 2005, *A&A*, 429, 791
- Quintana, H., & Lawrie, D. G. 1982, *AJ*, 87, 1
- Richstone, D. O. 1976, *ApJ*, 204, 642
- Richstone, D. O., & Malumuth, E. M. 1983, *ApJ*, 268, 30
- Rudick, C. S., Mihos, J. C., & McBride, C. 2006, *ApJ*, 648, 936
- Ryan, R. E. Jr. et al. 2007, *ApJ*, in press (astro-ph/0703743)
- Sandage, A., Binggeli, B., & Tammann, G. A. 1985, *AJ*, 90, 1759
- Schechter, P. 1976, *ApJ*, 203, 297
- Schombert, J. M. 1988, *ApJ*, 328, 475
- Seigar, M. S., Graham, A. W., & Jerjen, H. 2007, *MNRAS*, in press
- Sommer-Larsen, J. et al. 2005, *MNRAS*, 357, 478
- Spergel, D. N. et al. 2007, *ApJS*, 170, 377
- Staveley-Smith, L., Davies, R. D., & Kinman, T. D. 1992, *MNRAS*, 258, 334
- Thompson, L. A., & Gregory, S. A. 1993, *AJ*, 106, 2197
- Trentham, N., & Hodgkin, S. 2002, *MNRAS*, 333, 423
- Trentham, N., & Tully, R. B. 2002, *MNRAS*, 335, 712
- Trentham, N., Tully, R. B., & Mahdavi, A. 2006, *MNRAS*, 369, 1375
- Tyson, J. A. & Fischer, P. 1995, *ApJ*, 446, L55
- van der Marel, R. P., Magorrian, J., Carlberg, R. G.; Yee, H. K. C., Ellingson, E. 2000, *AJ*, 119, 2038
- Vilchez-Gomez, R. 1999, *ASPC*, 170, 349
- Waxman, E., & Miralda-Escude, J. 1995, *ApJ*, 451, 451
- Weil, M. L. et al. 1997, *ApJ*, 490, 664
- West, M. J. et al. 1995, *ApJ*, 453, L77
- White, S. D. M., & Frenk, C. S. 1991, *ApJ*, 379, 52
- White, S. D. M., Navarro, J. F., Evrard, A. E., & Frenk, C. S. 1993, *Nature*, 366, 429
- White, P. M., Bothun, G., Guerrero, M. A., West, M. J. & Barkhouse, W. A. 2003, *ApJ*, 585, 739
- Willman, B., Governato, F., Wadsley, J., & Quinn, T. 2004, *MNRAS*, 355, 159
- Xue, Y.-J., & Wu, X.-P. 2000, *MNRAS*, 318, 715
- Zibetti, S., White, S. D. M., Schneider, D. P., & Brinkmann, J. 2005, *MNRAS*, 358, 949
- Zwicky, F. 1951, *PASP*, 63, 61